Journal Pre-proof

Tunable formation of nanostructured SiC/SiOC core-shell for selective detection of SO$_2$

A. Gaiardo, B. Fabbri, A. Giberti, M. Valt, S. Gherardi, V. Guidi, C. Malagù, P. Bellutti, G. Pepponi, D. Casotti, G. Cruciani, G. Zonta, N. Landini, M. Barozzi, S. Morandi, L. Vanzetti, R. Canteri, M. Della Ciana, A. Migliori, E. Demenev

Please cite this article as: Gaiardo A, Fabbri B, Giberti A, Valt M, Gherardi S, Guidi V, Malagù C, Bellutti P, Pepponi G, Casotti D, Cruciani G, Zonta G, Landini N, Barozzi M, Morandi S, Vanzetti L, Canteri R, Della Ciana M, Migliori A, Demenev E, Tunable formation of nanostructured SiC/SiOC core-shell for selective detection of SO$_2$, *Sensors and Actuators: B. Chemical* (2019), doi: https://doi.org/10.1016/j.snb.2019.127485

This is a PDF file of an article that has undergone enhancements after acceptance, such as the addition of a cover page and metadata, and formatting for readability, but it is not yet the definitive version of record. This version will undergo additional copyediting, typesetting and review before it is published in its final form, but we are providing this version to give early visibility of the article. Please note that, during the production process, errors may be discovered which could affect the content, and all legal disclaimers that apply to the journal pertain.

Tunable formation of nanostructured SiC/SiOC core-shell for selective detection of SO₂

A. Gaiardo[1,*], B. Fabbri[2], A. Giberti[3], M. Valt[2], S. Gherardi[2], V. Guidi[2], C. Malagù[2], P. Bellutti[1], G. Pepponi[1], D. Casotti[2], G. Cruciani[2], G. Zonta[2], N. Landini[2], M. Barozzi[1], S. Morandi[4], L. Vanzetti[1], R. Canteri[1], M. Della Ciana[2,5], A. Migliori[5], E. Demenev[1]

[1] MNF - Micro Nano Facility, Bruno Kessler Foundation, Via Sommarive 18, 38123 Trento, Italy

[2] Department of Physics and Earth Science, University of Ferrara, Via Saragat 1/c, 44122 Ferrara, Italy

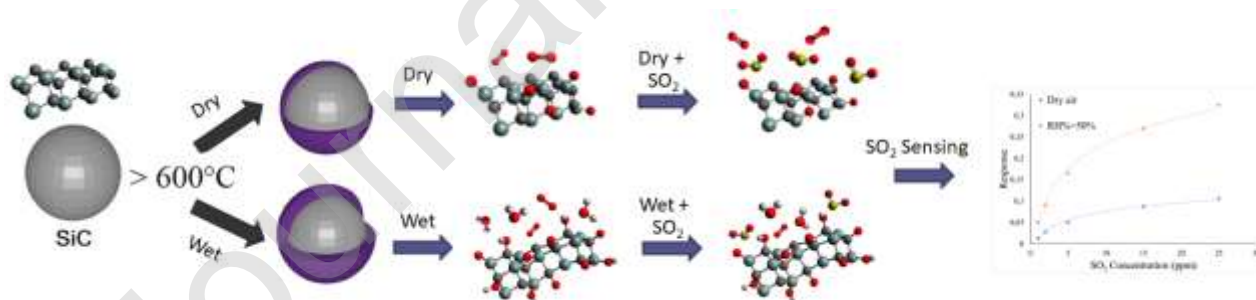[3] MIST E-R s.c.r.l., Via P. Gobetti 101, 40129 Bologna, Italy

[4] Department of Chemistry, INSTM and NIS Centre, University of Torino, via Quarello 15, Torino, I-10135, Italy

[5] Unit of Bologna, Institute for Microelectronics and Microsystems, National Research Council, via Gobetti 101, Bologna, 40129, Italy

_____

*   Corresponding author. Tel. +39 0461 314 451

        Email address: gaiardo@fbk.eu

Graphical abstract

Highlights

- In this work it was demonstrated that, under proper condition, it is possible to thermo-activate the surface reactivity of nanostructured SiC for the chemoresistive detection of gases.
- SiC gas sensors resulted to be an extremely selective functional material for the detection of sulphur dioxide (SO_2) in concentrations within the ppm range, both in dry and wet air. The presence of the humidity increased the gas sensing properties of SiC sensors vs. SO_2.
- The SiC surface reactivity vs. SO_2 is promoted by the formation of a SiC-SiOC core-shell, due to the thermal-oxidation of the SiC nanoparticle surfaces.

Abstract

Silicon carbide is a well-known material with high thermal, mechanical and chemical stability. These properties have allowed, over time, its wide use as an inert material to be employed as a substrate or support in different applications. In this work, we demonstrate that, under proper conditions, it is possible to activate the chemical reactivity of nanostructured SiC, which can be employed for chemoresistive purposes. With this aim, a commercial powder of SiC has been characterized from a morphological, structural and thermal point of view. Then, screen-printed thick films were obtained from SiC powder and thus tested as a functional material for chemoresistive gas sensors, in thermo-activation mode. The samples were exposed to 13 gases with important chemical differences. Analyses showed that SiC is an extremely selective functional material for the detection of sulphur dioxide (SO_2) in concentrations within the ppm range. This interesting result was found at high working temperatures (600-800°C), useful for harsh environments, and the measurements proved to be completely free from humidity negative interference. Thermo-gravimetric and X-ray photoelectron spectroscopy characterizations highlighted that the high selectivity of the SiC layer is promoted by the thermal formation of a SiC/SiOC core-shell, tunable by controlling temperature and humidity parameters. An interpretation of the gas sensing mechanism occurring between SO_2 molecules and SiC/SiOC core-shell has been proposed.

The unexpected chemical activity, identified for nanostructured SiC, can be exploited for the specific detection of SO_2, since this gaseous compound plays an important role in air pollution, industrial processes and winemaking.

Keywords: Chemoresistive gas sensor; SO_2 detection; nanostructured SiC thick film; SiC/SiOC core-shell; high selectivity.

2

1. Introduction

Nowadays, the accurate detection of pollutant gases is of fundamental importance for sustainable human development [1,2]. Indeed, several toxic gases at harmful concentrations for humans and dangerous for the environment are produced every day by industry emissions, farming, burning of fossil fuels and waste treatment [3]. In addition to these primary emissions, some pollutants (secondary emissions) can also be formed by the chemical interaction involving precursor substances [4]. As a result, despite the last agreements of the Nations Framework Convention on Climate Change (UNFCCC) on the greenhouse-gas-emissions mitigation, total gaseous emissions still have a strong negative impact on both the environment and the human health [5,6]. Among the various gaseous compounds, SO_2 is one of the major air pollutants worldwide [7]. The main anthropogenic sources of SO_2 include fuel combustion, power plants, industrial processes, residential coal combustion, natural gas pipelines and vehicle diesel engines, while the volcanic activity is the major natural contributor to these emissions [8-11]. The Threshold Limit Value Time-Weighted Average (TLV-TWA) of SO_2 is 5 ppm, because of its high toxicity for human health even in low concentrations [12]. Indeed, inhaled SO_2 can easily be hydrated in the respiratory tract, producing sulphurous acid that subsequently dissociates to form its derivatives, bisulfite and sulphite anions [13]. Furthermore, SO_2 is a systemic oxidative damaging agent [13]. Exposures to SO_2 produces different symptoms such as pneumonia, thickening of the mucous layer of the respiratory tract, nasopharyngitis, fatigability, asthma, gastritis, and alterations in the senses of taste and smell [13-17]. Further investigations evidenced the correlation between SO_2 exposition increase and the increment of the chronic obstructive pulmonary diseases and daily mortality [18-20]. Although the total anthropogenic emission of this gas has been decreasing in recent years, there are several areas of the world where emissions of SO_2 still represent a serious risk to human health [21-23].

For this reason, an increasing number of studies have been focused on the development of compact and portable gas sensors for the accurate detection of SO_2 [24-28]. Chemoresistive gas sensors have shown significant advantages among the various sensing devices investigated, such as rapid response, easy and low-cost fabrication [29,30]. Nevertheless, chemoresistive gas sensors are still poorly investigated in the detection of this gas since the low reactivity of SO_2 vs. oxygens adsorbed on the Metal-OXide (MOX) semiconductor surface, commonly used as sensing layer, results in difficult detection of SO_2 traces with respect to other typical sulphur gaseous compounds [29, 31-35].

In this work, the chemoresistive properties of nanostructured Silicon Carbide (SiC) to detect SO_2 have been thoroughly investigated, owing to good sensing capabilities shown by this material in

3

our previous work to selective detect SO_2 in the presence of H_2S [36]. So far, silicon carbide has been widely studied as a sensor device substrate due to its strong chemical and mechanical stability up to high working temperature [37-40]. Its high stability has led in several investigations to use SiC as an inert support for various nanostructured sensing materials, such as metal oxides, metals and polymers [41-48]. However, SiC can be also synthesized in the form of nanoparticles [49-52]. Among functional materials, nanostructured semiconductors are implemented for their electrical properties very different from single crystals, due to the major role that the surface potential plays in the conduction mechanism [53-55]. Furthermore, under proper operating conditions (thermo-activation or photo-activation), a nanostructured material highlights a high surface reactivity, which can be used to adsorb gaseous molecules or for heterogeneous catalysis [56-59]. In particular, chemoresistive gas sensors take advantage of this phenomenon, transducing variations of the chemical composition of the atmosphere into variations of the electrical resistance of a film composed by the nanostructured semiconductor [60-64]. To the best of our knowledge, only three papers are focused on the chemoresistive properties of pure nanostructured SiC. On the one hand, Sun et al. and Li et al. investigated the possible use of SiC nanosheets and SiC nanopaper, respectively, to detect humidity [65, 66]. On the other hand, Milanov et al. studied the sensing properties of electrochemically porosized SiC to detect ethanol [67]. Nevertheless, in none of these a detailed analysis is made on the sensing properties of the nanostructured SiC at different temperatures and in the presence of a wide selection of gases belonging from different chemical classes.

In this work, encouraged by the multiple fields in which SiC can be applied and by the possibility to have it in the form of a nanosized powder, we investigated in-depth its chemoresistive properties. A commercially available SiC nanosized powder was purified and characterized from the chemical, morphological and structural point of view. Subsequently, SiC thick films were tested as sensing layers for gas sensors, by exposing them to SO_2 and to other 12 gases belonging to different chemical classes, in thermo-activation mode. SiC layers turned out to be insensitive to almost all gas analysed, while showing a perfect selectivity to SO_2 in the concentration range of some ppm, in dry condition. Furthermore, the electrical characterization showed an increase in the response and in the cross selectivity to SO_2 in presence of humidity. This SiC behaviour was unexpected compared to common metal oxides, in which the presence of humidity represents a drawback, inducing a drastic decrease of the sensing response and of the sensitivity [68-70]. This result was obtained for high working temperatures (600°C), suggesting a potential use of this sensing material also in a harsh environment.

2. Experimental

4

2.1 Silicon Carbide powder treatments

The SiC nanopowder (Tec Star) datasheet reported an average grain size of 34 nm and a chemical degree of purity higher than 99%.

First, the commercial powder was treated to further purify it from contaminants. With this aim, 5 g of nanostructured SiC was washed several times by means of EBA 200 centrifuge at 6000 rpm for 15 minutes, by using both water and propanol. Afterwards, the powder was heated up at 650°C for 2 hours to remove possible organic contamination. Finally, SiC nanoparticle sizes were homogenized through a treatment in a Retsch bull mill (type MM 200), at 1500 rpm for 30 minutes

2.2 Characterizations

The X-ray diffraction analysis was performed in a Bruker D8 Advance diffractometer, equipped with a copper X-ray tube operating at 40 kV and 40 mA, and with a LINXEYE XE detector. The identification of the phases was achieved by the search-match routine implemented in the EVA v.14.0 program by Bruker with reference to the Powder Diffraction File database (PDF) v. 9.0.133. Quantitative phase and crystallite size were evaluated by the Rietveld method and the fundamental parameters approach for modelling the peak-profiles [71-73], using the TOPAS v.4.1 program by Bruker AXS [74]. The crystal size was calculated by the Double–Voigt approach [75], as volume-weighted mean column heights based on integral breadths of peaks.

The morphology and chemical composition of the SiC powder were analysed by Scanning Electron Microscopy and Energy Dispersive X-Ray spectroscopy (SEM-EDX spectroscopy) techniques, by means of a cold cathode JEOL Microscope, model JSM 7401-F.

A LabRam HR800 spectrometer (Horiba Jobin Yvon, France), coupled with an Olympus BXFM optical microscope (Olympus, Tokyo, Japan), was used for Raman characterizations. The instrument was equipped with air-cooled CCD detector (1024×256 pixels) set at -70 °C, and with 600 and 1800 grooves/mm gratings. The spectral resolution was approximately 4 cm^{-1} and the laser beam was concentrated in a spot with a diameter of 1 mm. The He–Ne laser line at 632.82 nm was used as excitation source and was filtered to keep the laser power varying from 0.2 to 10 mW. Exposure time, accumulations and beam power have been optimized for each sample to obtain sufficiently informative spectra and ensuring to avoid sample alterations.

X-ray Photoelectron Spectroscopy (XPS) analyses were performed using an ESCA 200 Scienta instrument equipped with a monochromatic Al Kα (1486.6 eV) x-ray source. For the measurements, the powders were attached to the sample holder using double-sided carbon tape. The emission angle between the axis of the analyser and the normal to the sample surface was 0°. For each sample, the

5

survey and high-resolution scans of the O 1s, C 1s and Si 2p core levels were collected. XPS quantification was performed using the instrument sensitivity factors and the high-resolution scans. Charge compensation was achieved using an electron flood gun and all core levels were referenced to the C-Si component in C 1s at 282.3 eV.

A Netzsch STA 409 (Netzsch Geraetebau, Selb, Germany) TG/DTA thermal analyser was used to perform the thermogravimetric analysis of the samples, equipped with a TG sample. For each measurement was used 40 mg of powder. The analyses were carried out under a constant air flow of 100 mL·min^{-1}, in the range 25-900°C, with a heating rate of 10 °C·min^{-1}. The same measurements were carried out both in dry and in wet air, by using a Drexler bubbling system filled with 200 mL of distilled water.

Microstructural and compositional analyses were performed by using a Philips TECNAI F20 ST transmission electron microscope (TEM) operating at 200 kV. The instrument was equipped with a dispersion micro-analysis of energy (EDS) and the scanning transmission (STEM) accessory. The TEM images were acquired in phase contrast mode. The samples were ground and suspended in isopropyl alcohol, then a few drops of the solution were evaporated on a copper grid coated with an amorphous carbon film.

The specific surface areas of the samples were determined by applying the Brunauer–Emmett–Teller (BET) method to the adsorption/desorption isotherms of N2 at 77 K obtained with a Micromeritics ASAP 2010 physisorption analyser.

2.3 Sensors preparation

The sensing paste was obtained by mixing organic vehicles with 1 g of SiC purified powder, to obtain a suitable paste viscosity [76]. The paste obtained was deposited onto alumina substrates by means of the screen-printing technique. The resulting deposition area for each sensor was 1.22x1.6 mm^2, with a thickness of about 20-30 μm [76]. The substrates were provided with both gold electrodes on the front-side, for measuring sensing material electrical properties, and heaters on the back-side, to set the temperature of the device [61, 77]. Substrates with SiC films were thermal stabilized at 180°C in a muffle for 4 hours, in order to evaporate the organic vehicles, and then fired at 650°C for 2 hours. Finally, the substrates were bonded on TO39 supports by using gold nanowire and connected to the measuring system [61, 63, 64].

2.4 Gas sensing measurements

The SiC sensors electrical conductance was measured in a dedicated gas test chamber. The conductance of the films was constantly collected during the gas sensing characterization through proper electronics, interfaced to a data-acquisition system [78, 79]. First, under a constant dry air flux of 500 sccm, the conductance values of the films were recorded changing the operating temperature in the range of 250-800°C, to evaluate the correlation between temperature and resistance of the sensing film.

Then, the gas sensing characterization was carried out. The sensors were kept at their working temperature and under a flow of synthetic air for few hours before the gas measurements, to allow the surface of the SiC grains to reach a thermodynamic steady state. Air and gases were fluxed into the test chamber from certified bottles by using a PC-driven mass-flow-controller. The electrical properties and the sensing performance of SiC films were deeply investigated through several different measurements. Gases belonging to different categories of molecules were chosen to test the surface reactivity of the semiconductor vs. gases with important chemical differences. Gas tests were performed with CO (10 ppm), propane (500 ppm), H_2S (10 ppm), NO_2 (5 ppm), acetaldehyde (10 ppm), acetone (10 ppm), ethanol (5 ppm), butanol (5 ppm), methane (1000 ppm), NH_3 (20 ppm), H_2 (20 ppm), methanol (5 ppm) and SO_2 (10 ppm). The concentrations of CO, propane, H_2S, NO_2, acetaldehyde, butanol, NH_3 and SO_2 have been chosen based on TLV-REL values [80], whereas, the concentrations of methanol, ethanol and acetone were chosen based on the human odour threshold. In the presence of each gas, the sensor performances were investigated at operating temperatures ranging from 250°C to 800°C. Sensors response is defined as:

$$R = \frac{G_{gas} - G_{air}}{G_{air}}$$

where G_{gas} and G_{air} are the conductance values in gas and in air, respectively. The tolerance in the gas sensing response can be ascribed to the reference resistance tolerance, corresponding to 5% [79].

The same measurements were performed in dry air carrier (20% of O_2 and 80% of N_2) and wet air carrier, by means of a bubbling system filled with deionized water [78, 79]. The temperature and the Relative Humidity (RH%) in the gas chamber were controlled with a Pt100 and an HIH-4000 Honeywell commercial sensor (accuracy $\pm$ 3.5%), respectively [61]. In dry air, the RH% measured was below 1%. The stability and repeatability of the sensor response were also investigated. Sensor responses vs. SO_2 concentrations were collected to define the calibration curve of a SiC-based sensor tested at its proper working temperature, in dry condition. Finally, a cross selectivity characterization was carried out to verify that the sensor/catalytic properties of the SiC film vs. SO_2 were not affected

7

by the presence of other possible interfering gases.

3. Results and Discussion

3.1 Chemical, morphological and structural characterizations

XRD measurements were performed both for the pristine and the treated SiC nanopowder (Figure 1). The phase composition analysis highlighted, for both powders, the presence of the cubic Moissanite 3C (Zb-type, s.g. F-43) as predominant crystal phase (about 75%). In the pristine SiC, two further phases have been found, i.e. SiC-RS-type (cubic phase, s.g. Fm-3m) and Moissanite 21R (trigonal phase, s.g. R3m), with a concentration of 2% and 24%, respectively. In the treated sample, as it can be seen in Figure 1, the peaks of SiC-RS-type phase disappear, and the concentration of Moissanite 3C and Moissanite 21R were of 76% and 24%, respectively. The slight difference between the two samples is probably due to the washing-thermal processes applied to the treated SiC. The average crystallite size was about 21 nm in both samples.
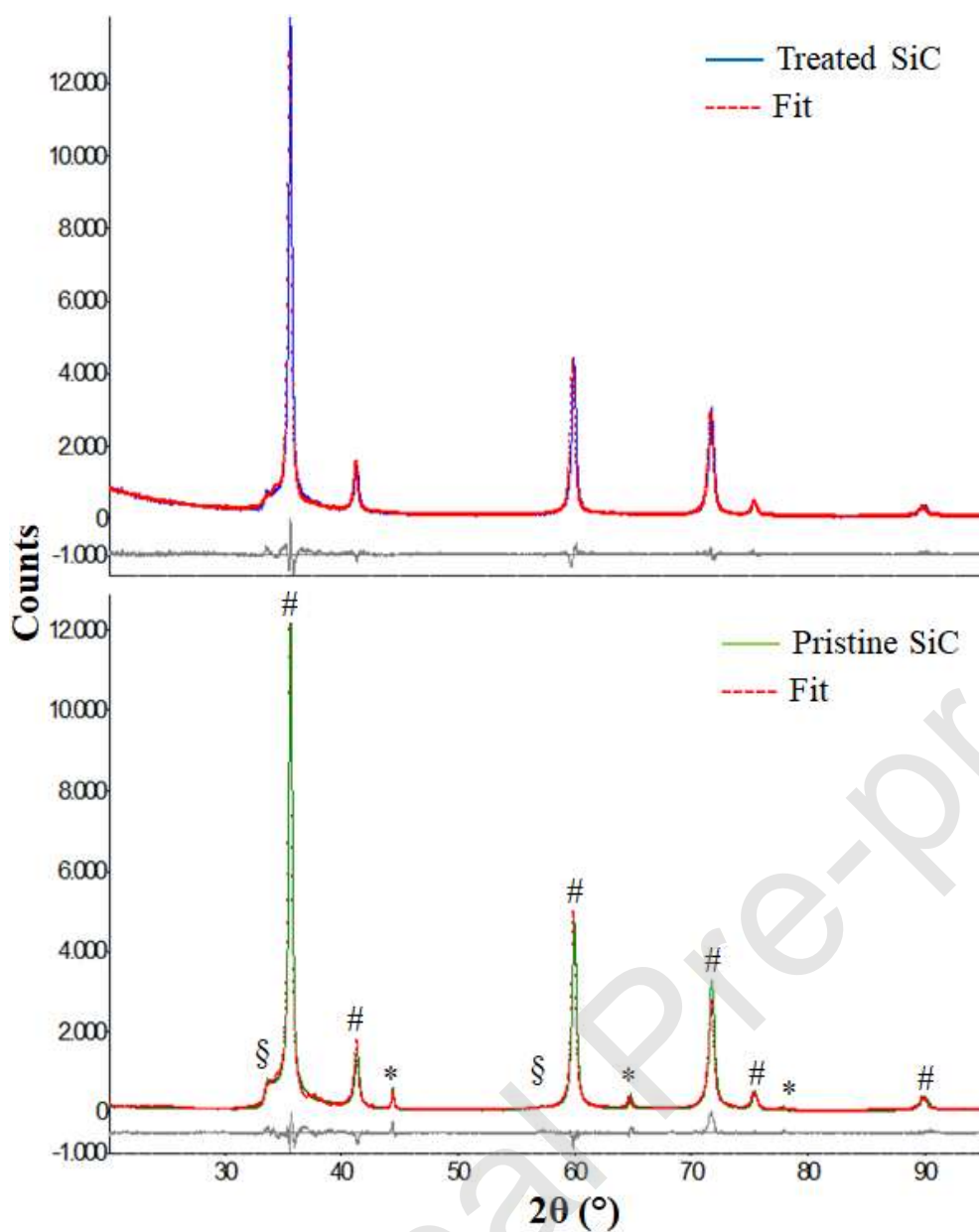
Figure 1: XRD patterns of the SiC nanopowder are reported in blue and green lines for the treated and pristine samples, respectively. The dashed red lines are the Rietveld fit. The identification of the phases showed the presence in the pristine sample of (#) Moissanite 3C; (*) SiC-RS-type; and (§) Moissanite 21R. The SiC-RS-type phase disappears in the treated sample.

The SEM characterization, performed for the treated powder, is shown in Figure 2. The analysis highlighted that the morphology of SiC grains was spherical-like, with an average size of tens of nanometers.
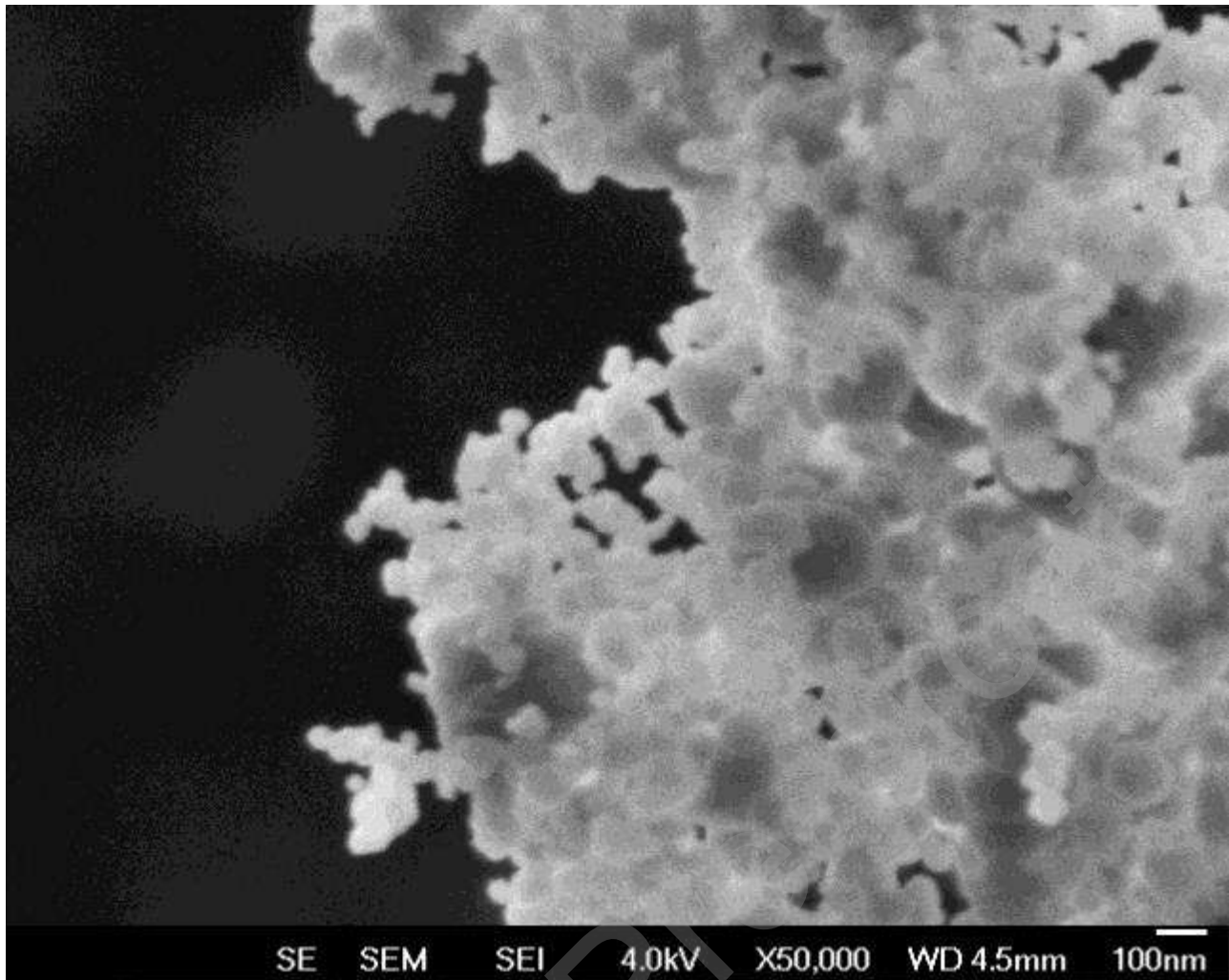
9

Figure 2: SEM image of the treated SiC nanopowder.

EDX analyses were carried out by using both silicon and carbon-tape substrates. The average atomic concentrations, investigated by using both substrates, are reported in Table 1.

Table 1: Average atomic percentages of elements found through EDX analyses.

C (at%)	O (at%)	Si (at%)
51.9 ± 14	6.1 ± 2.5	41.2 ± 16.2

It can be noticed that the SiC sample showed a high chemical purity, within the instrumental error. The Raman characterization, showed in Figure 3, was performed on the pristine SiC, and on the SiC nanopowder after the purification process.
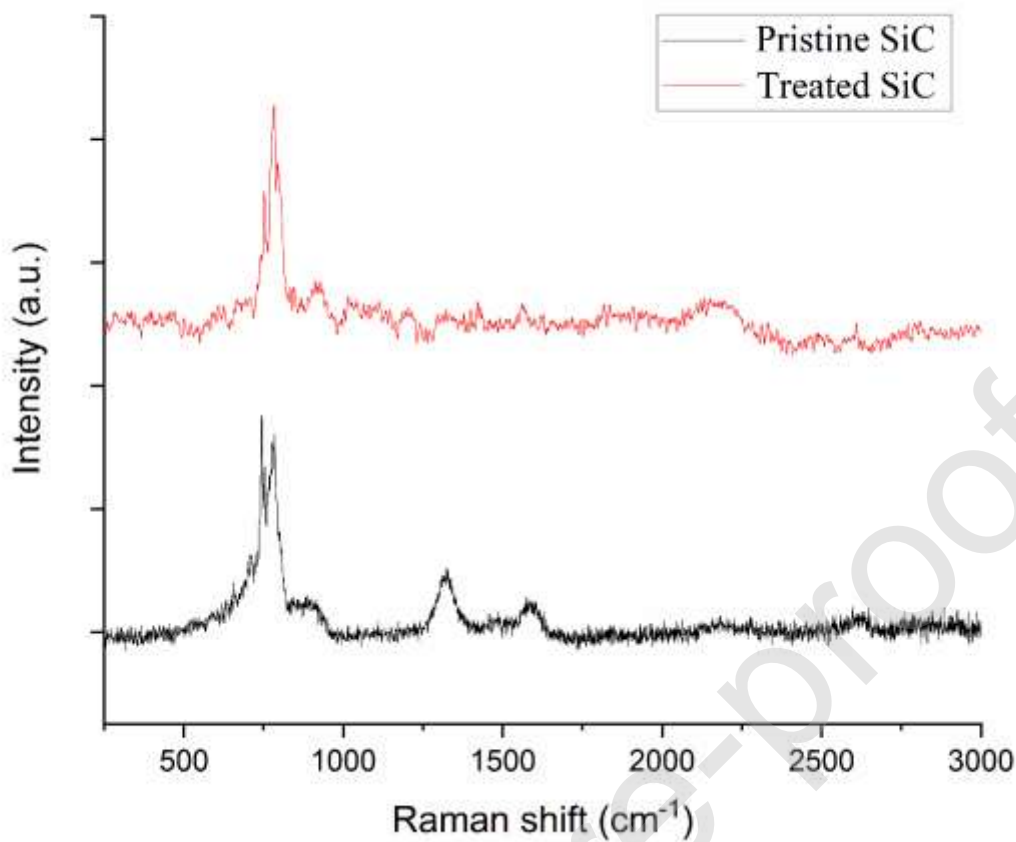
10

Figure 3: Raman spectra of pristine (dark line) and treated (red line) SiC samples.

There are four main peaks in the pristine SiC spectra (black line). Peaks located between the 700 cm$^-$^{1} and 1000 cm^{-1} are related to the presence polytypes in the SiC nanopowder, as also observed in the XRD characterization (Figure 1) [81]. The peak centered at 790 cm^{-1} can be attributed to the lattice vibration of the material, specifically to the zone-center transverse optical (TO) phonons of 3C-SiC [82]. The longitudinal optical phonon mode (LO) is shown with a Raman shift at 915 cm^{-1}, already observed by Parida et al. for SiC nanoparticles with an average size of 50 nm [83]. Two main characteristics bands are centered at 1334 cm^{-1} (carbon D band) and at 1595 cm^{-1} (carbon G band), which correspond to the vibrational properties of isolated carbon arrangements and sp^3 carbon bonding coming from surface atoms [82, 84, 85]. They can be attributed to the presence of a carbon-rich phase located outermost SiC nanoparticle surface or free carbon [82, 84-86]. A presence of a higher concentration of carbon than silicon in the SiC pristine sample was also observed through the EDS (Table 1) and XPS (Table 3) characterizations.

The spectra of the treated SiC nanopowder is shown in Figure 3 with the red line. On the one hand, the peaks related to TO and LO phonons of SiC polytypes are still detectable. On the other hand, the

11

D and G bands of the C-C bonds almost vanished, blending in with the background noise. The disappearance of such peaks could be attributed to the oxidation of the SiC nanoparticle surface due to the heat treatment at 650°C carried out in the purification process [85, 86]. The oxidation of the SiC nanoparticles surface will be discussed in a dedicated section (section 3.3, Gas sensing mechanism), owing it plays a key role in the SiC gas sensor performance.

3.2 Gas sensing results

In order to investigate the gas sensing properties of SiC thick films, the sensors were designed as reported in paragraph 2.3.

Firstly, it was investigated the relationship between the conductance of SiC screen-printed layer vs. temperature. Figure 4 shows average conductance values obtained for SiC thick films investigated. One can observe a very low conductance at low temperature, with an average value of 0.127 nS at 250°C. The film conductance increased with an exponential trend when the temperature increases, reaching 2.13 nS at a temperature of 800°C.
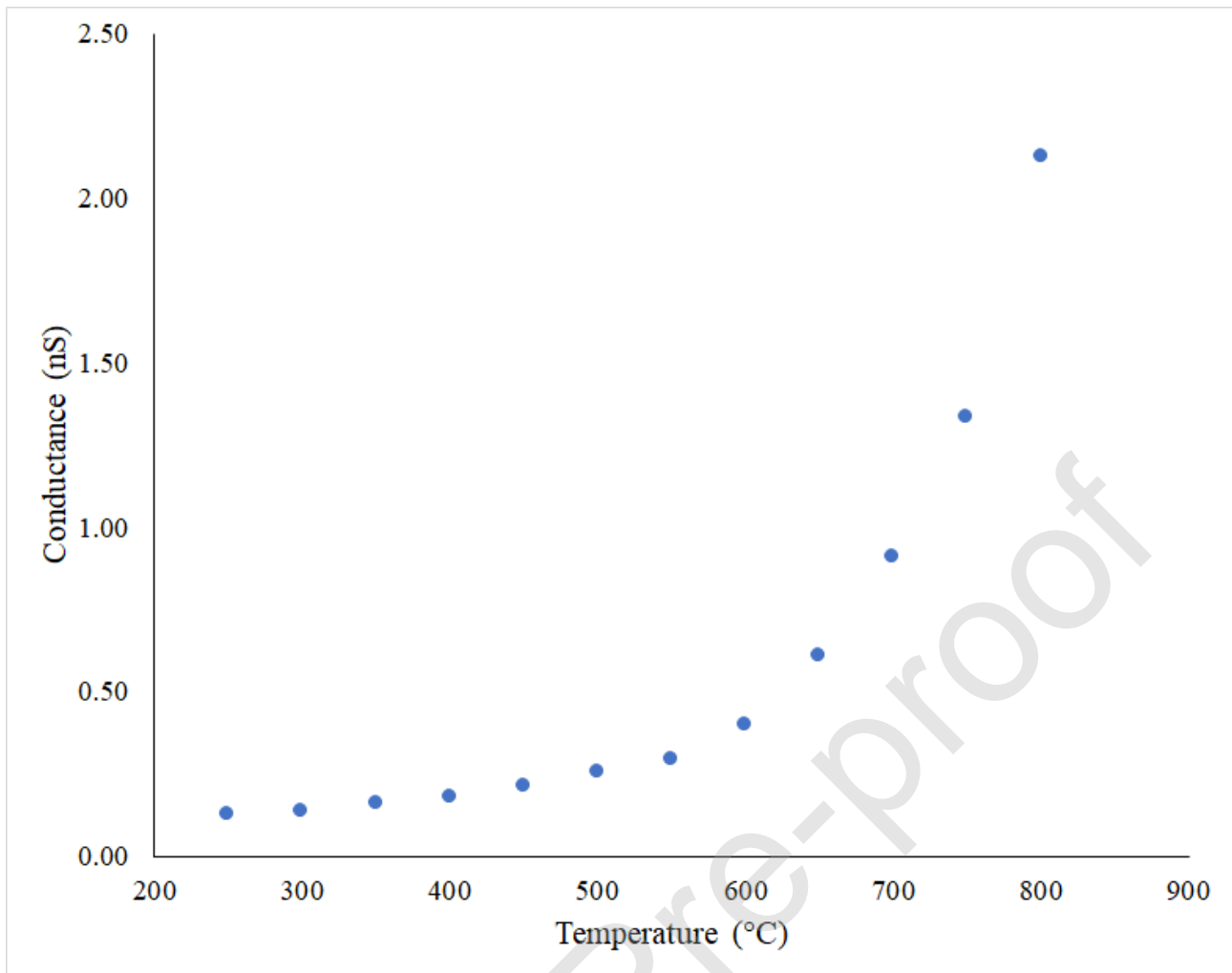
Figure 4: Plot of working temperature vs. SiC thick-film conductance. The tolerance for the sensor conductance is considered 5%, as explained in the section 2.4.

After the evaluation of SiC thick films conductance vs. temperature, their gas sensing properties were studied.

The gas sensing characterization was carried out both in dry and in wet air, at a working temperature ranging from 250°C to 800°C. Temperatures higher than 800°C were not investigated because most of the alumina substrates were broken at this temperature.

The measurements highlighted that SiC layer resulted to be insensitive, from a chemoresistive point of view to all gases tested, up to the working temperature of 600°C in dry air and 550°C in wet air, respectively. In Figure 5, summary graphs of SiC sensor sensing responses are reported, both in dry air (Fig. 5a) and in the presence of 13% of RH% (Fig. 5b).
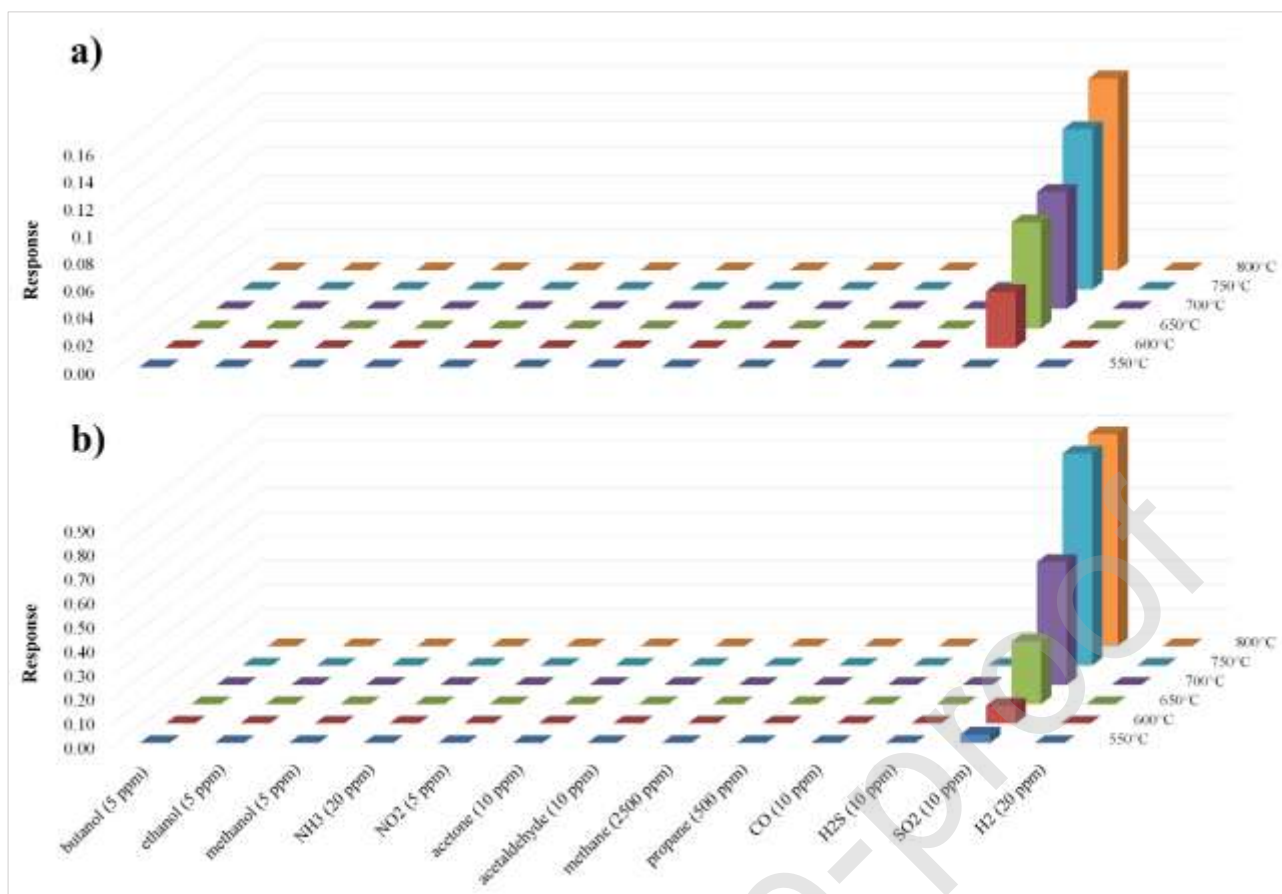
13

Figure 5: Summary histograms of SiC sensor responses vs. gases tested at different working temperatures, in **a)** dry air and **b)** in presence of 13% of RH%.

As it can be seen from Figure 5, the SiC layer did not highlight any change in conductance in the presence of almost all gases tested in dry air, except for SO_2, tested at a concentration of 10 ppm. Indeed, when exposed to this gaseous molecule, silicon carbide-based sensors showed a detectable and reversible change in conductance starting from a working temperature of 600°C, in dry air. The sensing response to 10 ppm of SO_2 increased at working temperatures higher than 600°C, as is shown in Figure 5a. The sensing behaviour of SiC thick film was also investigated in wet air, in order to study the sensing properties of the sensor in environment closest to real sensing applications, where humidity is the most common interfering gas [87]. The summary of the results obtained in the presence of 13% of RH% is reported in Figure 5b. The behaviour of the sensing material was the same as that observed in dry air, showing a detectable change in conductance only in the presence of 10 ppm of SO_2. However, the minimum working temperature useful to detect 10 ppm of SO_2 was lower in the wet air than in dry air (550°C in wet air vs. 600°C in dry air). Moreover, values of sensing responses vs. 10 ppm of SO_2 were higher in the wet air than in dry air for all the working temperatures where a conductance change was detectable. Thus, contrary to the typical behaviour of metal oxides, commonly used as chemoresistive gas sensors [88], the presence of humidity seems to improve the

14

sensing performance for SiC films, maintaining the selectivity vs. SO_2 and increasing the response value to this analyte.

Based on the data obtained, it was decided to carry out further sensing characterizations at a working temperature of 650°C, that was the temperature that highlighted the best compromise between SiC sensing properties and a reasonable condition to maintain the stability of the alumina substrate and the electronic system.

To deeply investigate the humidity influence on the sensing properties of SiC sensors, the sensing characterization of SiC films to 10 ppm of SO_2 at various percentages of RH% was performed. The dynamic responses obtained are reported in Figure 6.
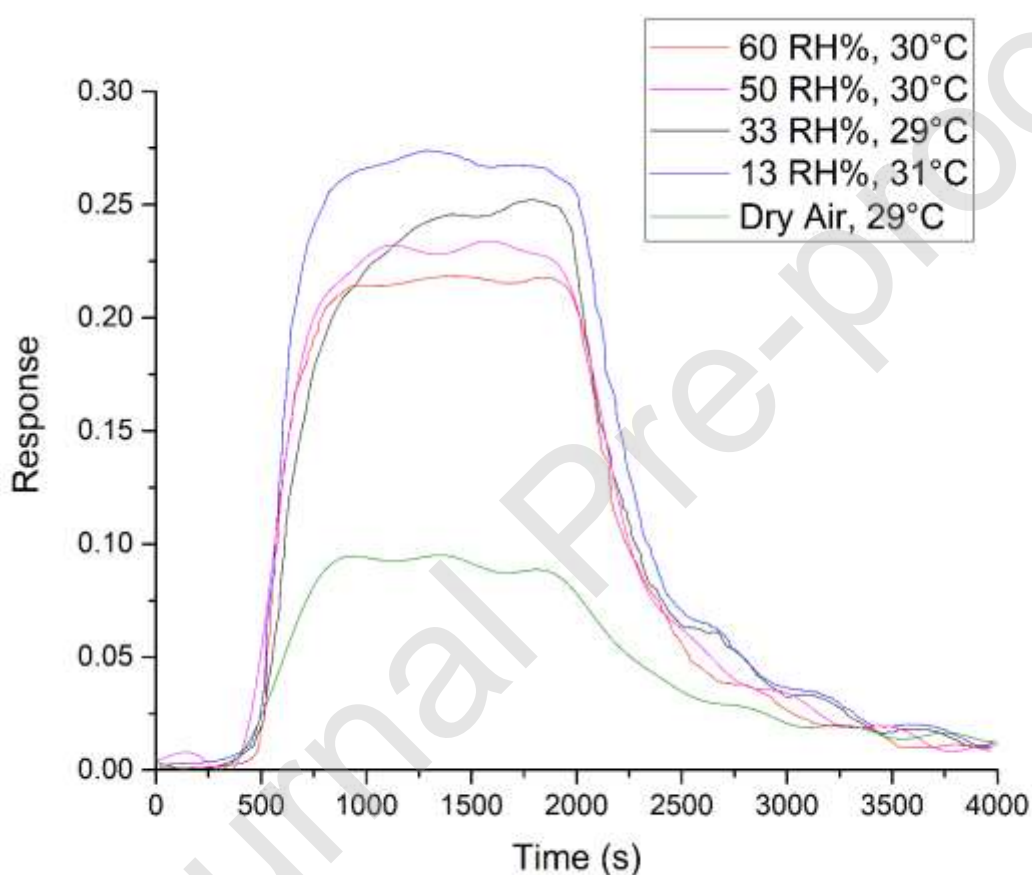

Figure 6: Dynamic responses of SiC sensors vs. 10 ppm of SO_2 in the presence of different RH% conditions.

As can be seen, all response values in wet air were higher than the response in dry air. The maximum response was recorded with 13% of RH%, while, with higher percentages of RH% the response slowly decreased, but they were still higher than the response obtained in dry air. This is counter tendency with respect to the behaviour of metal-oxide-based chemoresistive gas sensors, in which the humidity interacts with the film surface, occupying and thus decreasing possible reactive sites of the same metal oxide, resulting in a decrease of the sensing response compared with that in dry air [68,

15

69, 89]. The response and recovery times vs. 10 ppm of SO_2 were also investigated, since they are useful parameters both for the gas sensor application and to study the heterogeneous reaction kinetics occurring between the sensing material and the gas analysed [90, 91]. The values of response and recovery times are appropriate especially for comparing sensing materials measured in the same measuring chamber, since they are strongly dependent on the size and geometry of the chamber and the speed of the gas flow. In this work, the response time was calculated as the time that the sensor used to keep the 90% of the response [92], while the recovery time was calculated as the time that the sensor needed to switch back to 1/e of the response value. Results obtained are reported in Table 2.

Table 2: Summary table of recovery and response times of SiC sensors vs. 10 ppm of SO_2 in presence of different RH% values.

Relative Humidity (%)	Response Time (s)	Recovery Time (s)
Dry air	300	590
13	259	391
33	435	329
50	302	347
60	318	381

On the one hand, the response time resulted to be not related to the humidity presence. On the other hand, the recovery times, were lower in the presence of humidity than in dry air. Therefore, the presence of humidity affected both response value and time of reaction. These data highlighted that the presence of humidity probably modified the reaction kinetic between SO_2 and the surface of the SiC layer.

To investigate the repeatability of the SiC sensor, the device was exposed to SO_2 at a fixed concentration of 10 ppm. Figure 7 shows sensing responses by exposing the sensor to 4 cycles of SO_2 adsorption/desorption, at different RH% values.
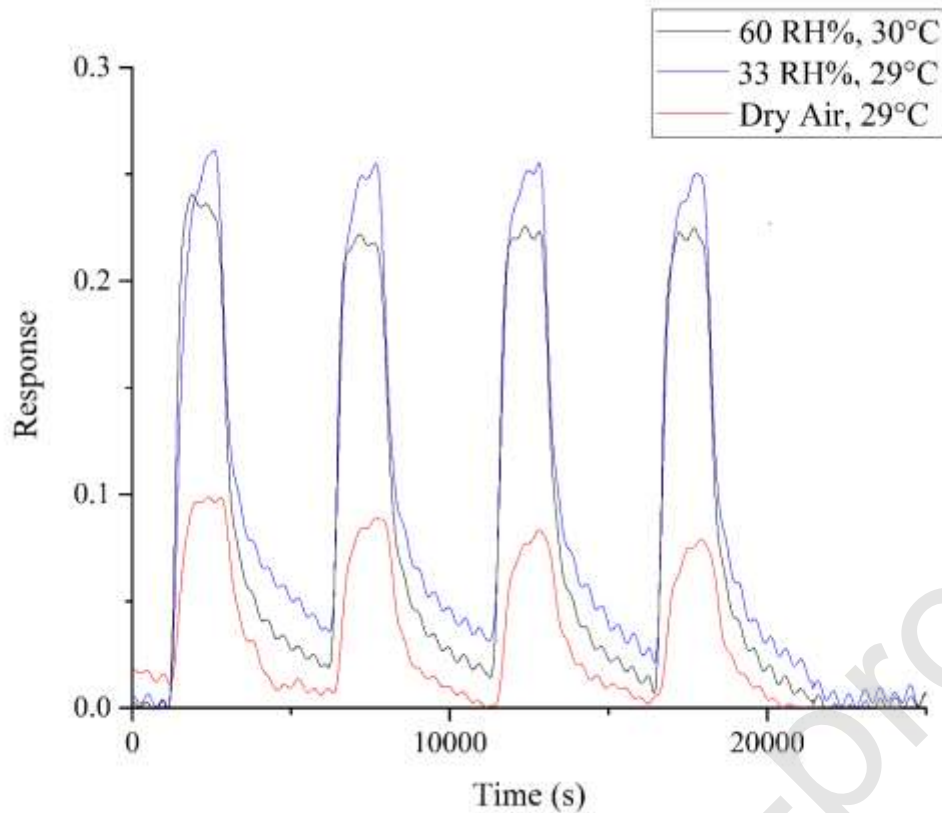
Figure 7: Stability of SiC sensors responses vs. 10 ppm of SO_2 at different RH%.

SiC sensors showed a repeatable and stable response in the range of hours, especially in wet condition. The last sensing parameter investigated of SiC device was the sensitivity, represents by the slope of the calibration curve [93]. To this aim, the SiC sensing response vs various SO_2 concentrations, i.e. 1, 2, 5, 15 and 25 ppm, was analysed. The data obtained in dry air and in wet condition (at a RH% of 50%, chosen as the common RH% level in outdoor conditions) are illustrated in Figure 8. The measurements have highlighted that the trend of the calibration curve is in line with the trend of the common metal-oxide gas sensors, with a decreasing of SiC sensor sensitivity for an increasing of the SO_2 [89].
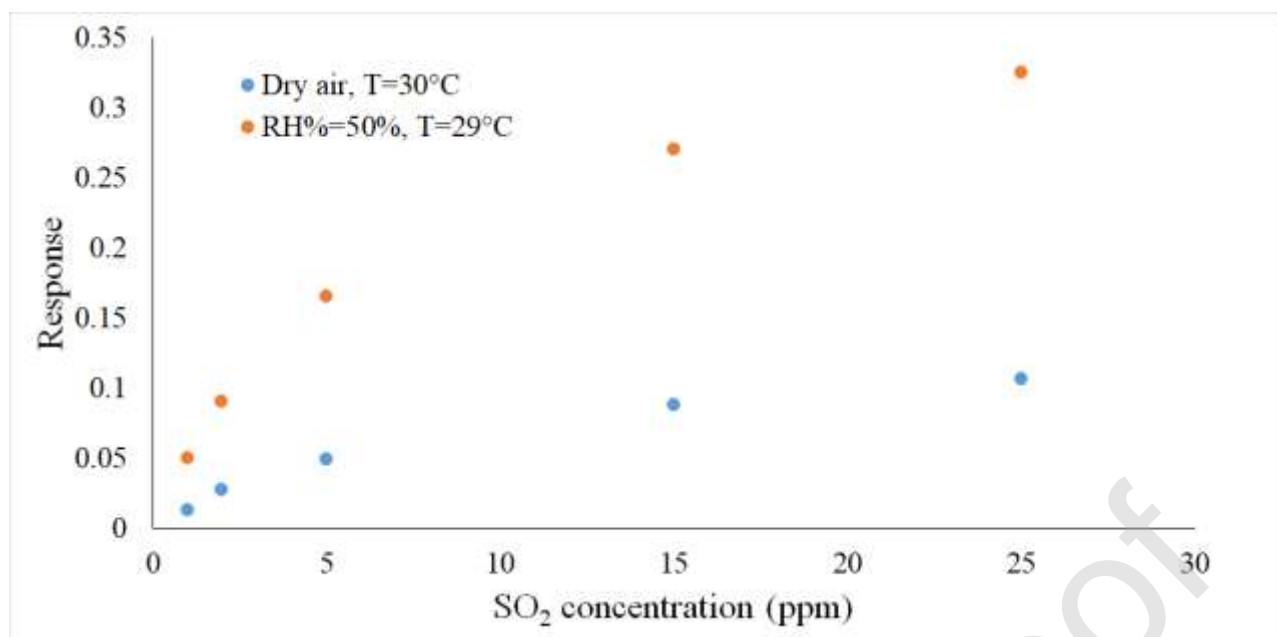
17

Figure 8: Calibration curves of SiC sensor vs. 1, 2, 5, 15 and 25 ppm of SO_2 at 650°C, in dry air (blue markers) and in presence of 50% of RH% (orange markers). A tolerance of 3% is considered on x-axis, given by the combination of tolerance of the SO_2 concentration in the cylinder and the tolerance of mass flows used. For Y-axis, 5% assigned as percentage error as reported in the section 2.4.

The lower detection limit identified at 650°C for SiC sensors was 1 ppm of SO_2, a useful concentration for gas application since it is two times lower than the Time-Weighted Average (TWA) exposure limit and 5 times lower than the Short-Time Exposure Limit (STEL) [80].

The possible cross-selective property of the SiC thick film was also investigated. The sensor was exposed to 10 ppm of SO_2 and then, in the gas chamber, other four different gases were injected in sequence, as reported in Figure 9.
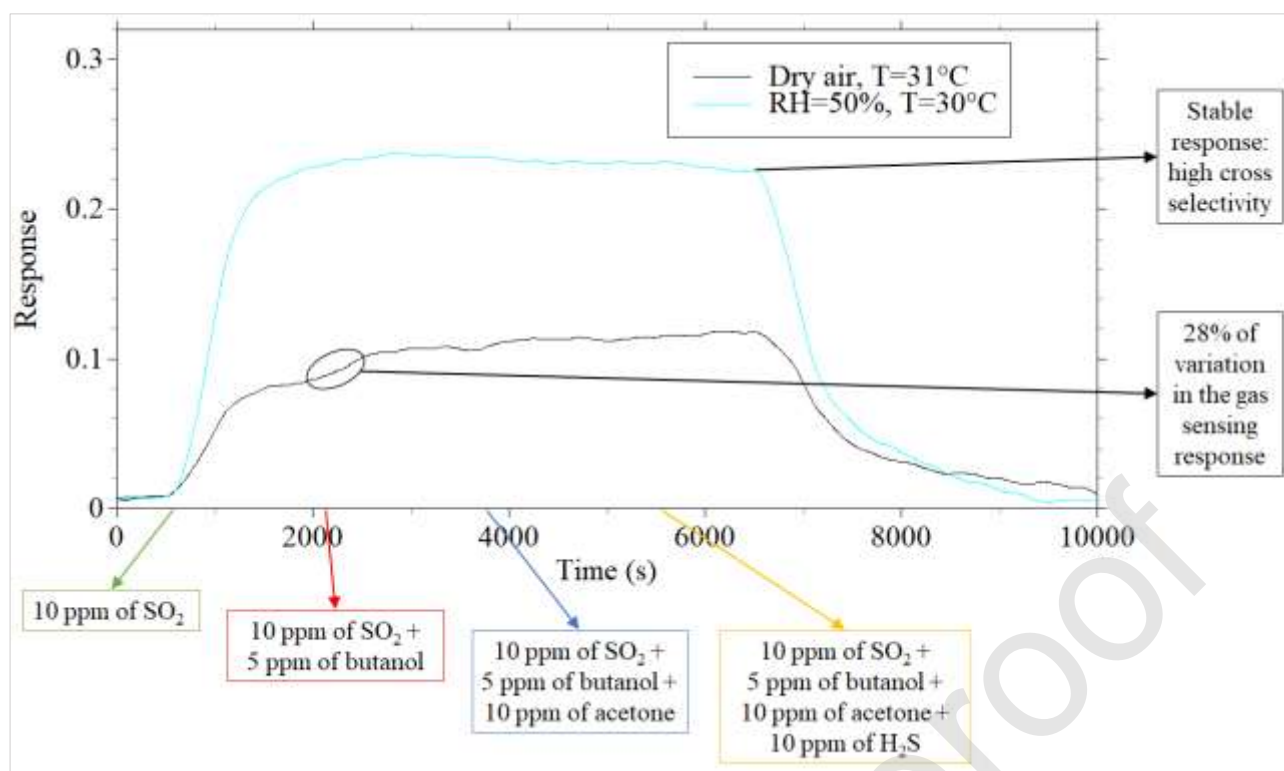
Figure 9: Cross selectivity analysis of the SiC sensor vs. 10 ppm of SO_2 at 650°C (50% of RH%) verified in presence of 5 ppm of butanol, 10 ppm of acetone and 10 ppm of H_2S.

As possible interfering species butanol and acetone were chosen, which are usually gases that strongly react with chemoresistive sensors, and H_2S since it is one of the most common interfering in applications where sulphur dioxide is present [94]. This characterization highlighted a great cross selectivity of SiC sensor in wet condition; meanwhile, an influence of 28% in the sensing response was detected in presence of 5 ppm of butanol in dry air. Since common applications of a gas sensor are in presence of humidity, the high cross selectivity shown by SiC highlights its possible specific use to detect SO_2 in real applications, such as air pollution and industrial processes gas analysis.
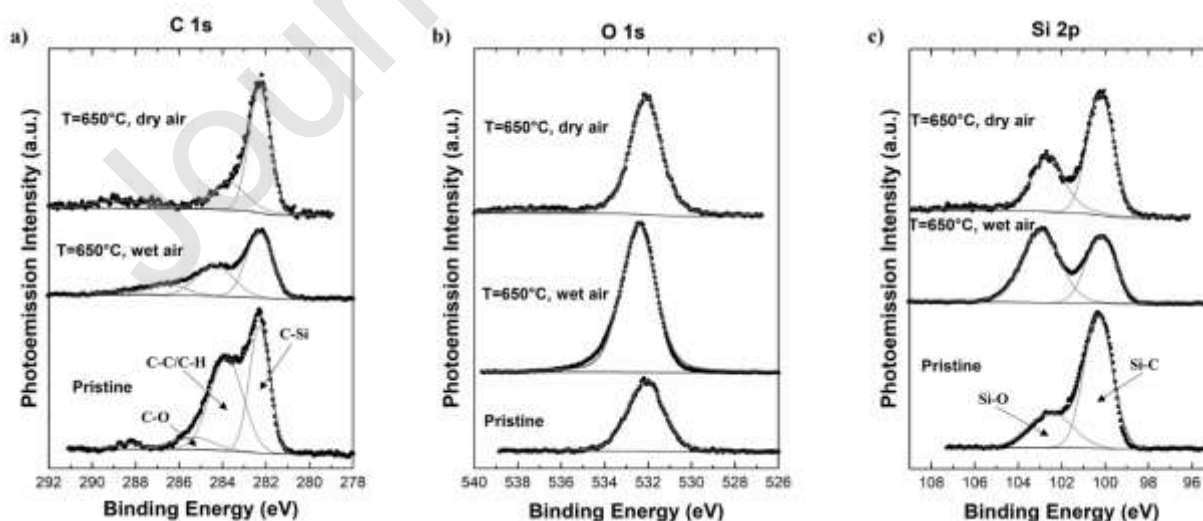
3.3 Gas sensing mechanism

As showed in the previous discussion, SiC sensor exhibited an increase reactivity to SO_2 by increasing the layer working temperature, until reaching a strong selectivity at temperature higher than 600°C. To better understand the sensing behaviour of SiC thick films, XPS analyses were conducted with the aim to detect possible composition change on the surface of SiC nanoparticles at high temperatures. XPS measurements were performed on three samples, the pristine SiC powder and the SiC powder after a heat treatment at 650°C in a furnace, under a constant flux of both dry and wet air. It is clear that, after heat treatments, there is a large increase in oxygen content in the SiC powder and a large decrease of the carbon concentration. Data of atomic percentage in the three samples are reported in

19

Table 3.

Table 3: Atomic content of oxygen, carbon and silicon obtained by means of XPS analysis for the three different SiC samples.

Sample	O (%)	C (%)	Si (%)
Pristine SiC	21.1	46.0	32.9
SiC 650° wet air	44.2	25.4	30.4
SiC 650° dry air	33.5	31.2	33.3

This increase in oxygen concentration could be ascribed to the oxidation of the SiC nanoparticle surfaces at high temperature, which allows the formation of a SiOC shell on the nanoparticles [95]. By analysing the C 1s, O 1s and Si 2p peaks and the related fit (Fig. 10), it can be observed that SiC oxidation increased in the wet heat treatment compared to the dry one. Regarding C 1s (Fig. 10a), it can be noted that the peaks related to the C-Si (282.3 eV) and C-C/C-H bonds were predominant in the pristine sample, and there was only a slight component due to the C-O bond. The ratio between C-Si and C-C/C-H peaks is strongly enhanced in the sample treated at 650°C in dry air, highlighting an increase of the C-Si component in the SiC powder. The sample treated in wet showed a preponderant increase of the peak due to the C-O bond compared to the other two samples. Concerning O 1s (Fig. 10b), it can be noted that heat treatments in dry and wet conditions moved it to higher energies than the pristine sample. This shift could be motivated by an augment of the O-Si component compared to the O-C one during the oxidation process [96], and by the increase of the oxidized layer on the SiC nanoparticle surfaces. As far as silicon is concerned (Fig. 10c), from the fit it can clearly be observed that the peak of the Si-O bond increased, due to heat treatments, to the detriment of the Si-C peak.

Figure 10: XPS analysis of **a)** C 1s, **b)** O 1s and **c)** Si 2p binding energy of the three SiC samples: Pristine SiC and SiC

20

heated at 650°C for 2 hours both in dry air and in wet air. Thick dashed lines are related to the spectra experimental data, meanwhile grey thin lines are the fit.

The experimental results obtained are in line with those reported in the literature. Indeed, several works have demonstrated, both experimentally and theoretically, the thermal surface oxidation of SiC nanoparticles due to the interaction between grains surface and O_2 or H_2O gaseous molecules [97, 98]. Among the different parameters that regulate the kinetics of oxidation, the most important are the grain size, the temperature and the moisture content. Roy et al. showed that the presence of H_2O molecules in the furnace environment increases the oxidation of the SiC nanoparticles [98]. This may explain the presence of a higher oxygen percentage in the SiC sample heated in the presence of humidity (Table 3).

A thermogravimetric analysis was also performed to deeply investigate the oxidation process that occurs in the SiC powder used in this work, both in dry and wet air. In Figure 11 the TG analysis, performed by using the commercial powder after washing cycles, as reported in the paragraph 2.1, but without the heat treatment, are shown. The two TG curves showed some differences. In dry air, no significant changes occurred to the material up to about 600°C, where a weight increase was detected, which continued up to 900°C with an exponential trend. Concerning the TG curve in wet air, it should be noticed that a slight weight increases in the SiC sample has already been identified from a temperature of 400°C. Then, a higher increase of the SiC powder weight starting from about 600°C up to 900°C with an exponential trend was observed.

The TG characterization confirmed the results obtained with the XPS analysis. Moreover, TG analysis demonstrated that the oxidation of the SiC nanoparticle surfaces is temperature dependent and the oxidation rate improves when the temperature increases, both in dry and in wet air [98]. The oxidation temperature, which depends on the particle size of the SiC, is in line with values reported in the literature for the SiC sample heated in dry air [99]. The motivation behind the higher weight increases in wet than in dry air can be attributed to the better oxidation of SiC nanoparticles in presence of H_2O molecules at high temperatures [98, 99].
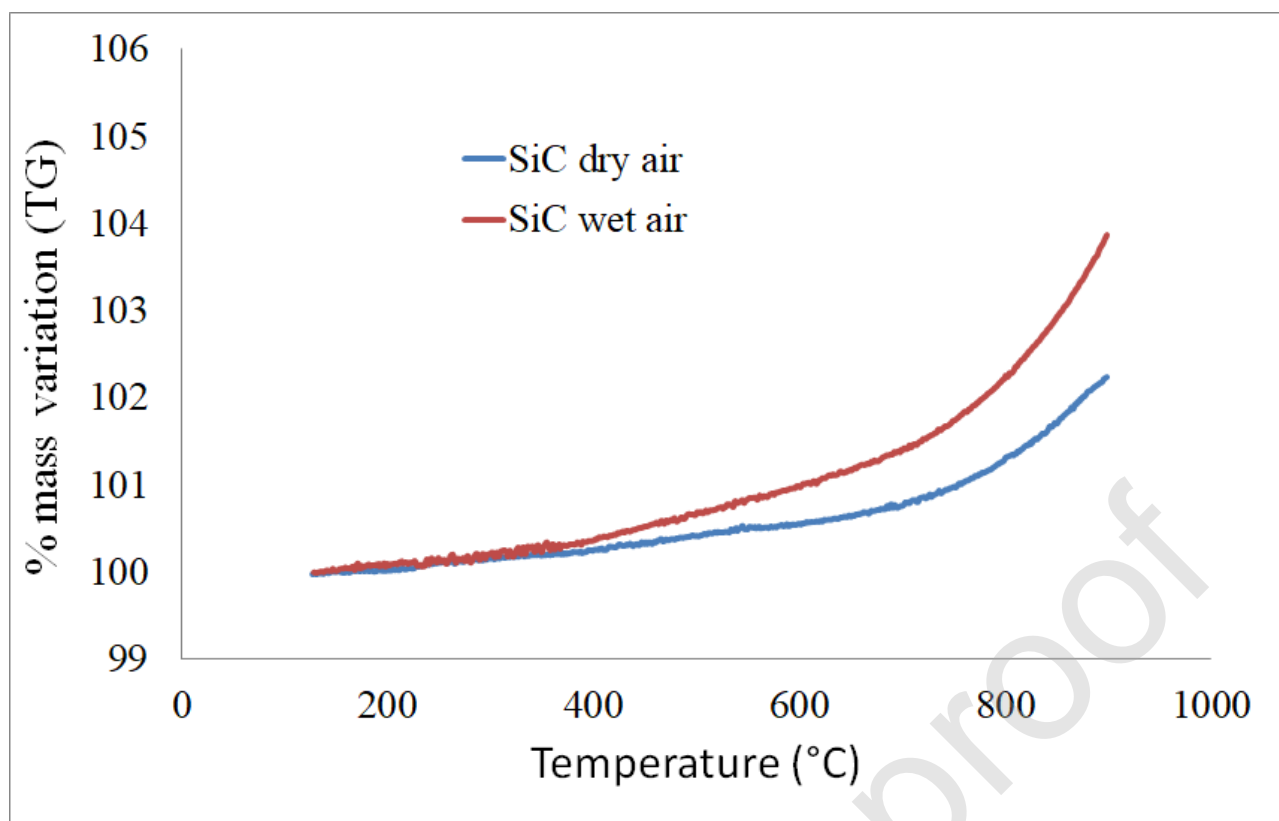
Figure 11: TG analysis of SiC powder in dry (blue line) and wet air (red line).

A TEM analysis was performed to obtain compositional (EDS) and structural information of the SiC nanoparticles surface, to deeply investigate the SiC/SiOC core-shell formation at high temperatures. Three different SiC samples were analysed, i.e. pristine SiC, SiC thermal treated at 650°C and at 850°C, in ambient air.
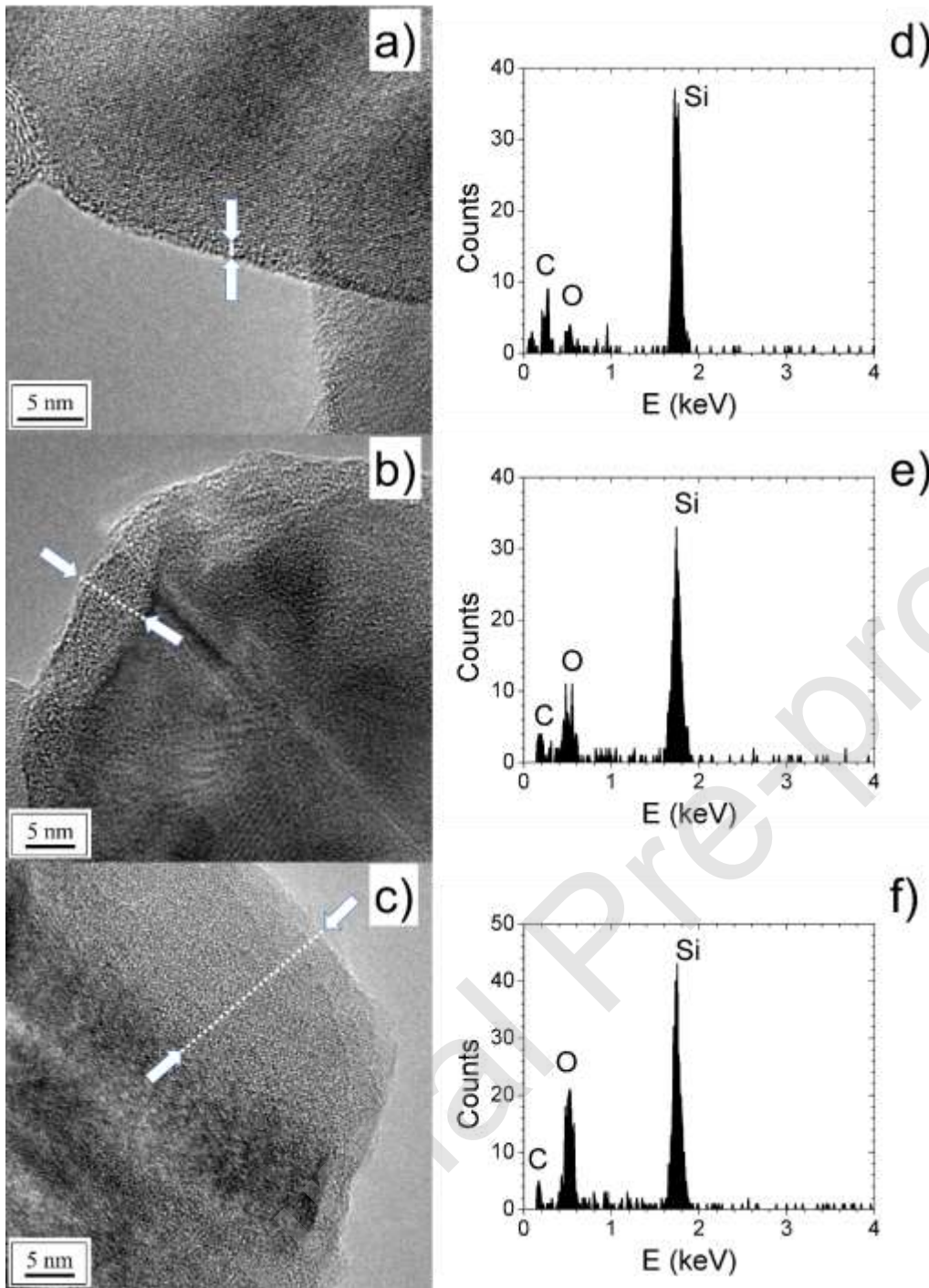
22

Figure 12: a, b, c) High Resolution TEM (HRTEM) images, **d, e, f)** EDS compositional analysis of nanoparticle surfaces of the pristine SiC, SiC thermal treated for 2 hours at 650°C and 850°C, respectively.

As it can be observed in Figure 12, nanoparticles of the pristine SiC (Figure 12a) are surrounded by a thin amorphous layer of about 0.5 nm, due to the formation of the native oxidation layer. In Figures 12b and 12c, it is clear that the thermal treatments strongly increase the thickness of the amorphous layer on the SiC nanoparticles, which was about 5 nm for the SiC sample treated at 650°C and about 10-15 nm for the one treated at 850°C.

Figures 12d, 12e and 12f show EDS analyses of the three samples, carried out by investigating the

compositional profile of the SiC nanoparticle surface. The analysis revealed that, in the limit of the spatial resolution, there is an increase in the oxygen content on the surface of SiC nanoparticles, related to the thickness growth of the amorphous layer that surrounded the same nanoparticles after the heat treatment at 650°C and at 850°C.

Therefore, results obtained through TEM images and EDS compositional analysis support data obtained with the TG and XPS analyses, highlighting the formation of the SiC/SiOC core-shell at high temperatures, caused by an oxidation of the SiC nanograins' surface [95]. Furthermore, the TEM analysis shown that the SiOC shell formed on the SiC surface is amorphous.

The sensing property improvement at high temperature of SiC sensor could be attributed to the SiC/SiOC core-shell formation. Indeed, TG analysis highlighted a weight increase occurred at about 600°C in dry air and at temperature lower than 600°C in wet air, respectively, due to surface oxidation of SiC nanoparticles. These coincide with the temperatures at which SiC thick films started to exhibit reactivity to SO_2. Many works in the literature highlight how core-shell of composite materials enhances chemical, physical and optical properties than individual materials studied separately [100]. Furthermore, although SiC has always been considered an inert material with high chemical stability, Karakuscu et al. have demonstrated that mesoporous SiOC glasses show sensing properties under proper condition [101]. The possible high concentration of defects in the SiOC shell, obtained through thermal oxidation, could be an additional factor in increasing the surface reactivity of the SiC/SiOC core-shell [102]. The surface reactivity boosted by the formation of the SiC/SiOC core-shell would also explain the better sensing properties showed by SiC layers in wet than in dry air. In fact, the presence of moisture supports the surface oxidation of SiC nanoparticles, promoting the formation of the core-shell and therefore both the reactivity and the selectivity of the SiC film vs SO_2 molecules (see Figure 9).

The high temperature is however essential to keep the surface active for the interaction with SO_2 from a chemoresistive point of view, even after the formation of the of the SiC/SiOC core shell. In fact, further electrical characterizations have shown that, using the material after the formation of the core-shell, SiC sensors did not show measurable changes in conductivity during exposure to SO_2 at temperatures below 600°C in dry air and 550°C in wet air, respectively.
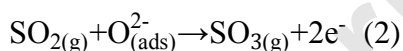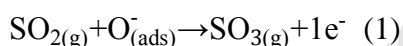
The surface area of the SiC nanopowders were determined by applying the Brunauer–Emmett–Teller (BET) method, in order to investigate its variation due to the SiC/SiOC core-shell formation. Four different samples were analysed, i.e. pristine SiC, SiC thermal treated at 400°C, 650°C and 850°C, in ambient air. The surface areas were reported in Table 4.

24

Table 4: BET surface area values for the pristine SiC, and for the SiC nanopowder calcined at 400°C, 650°C and 850°C.

Sample	BET surface area (m^2/g)
pristine SiC	21.4277 ± 0.0473
SiC calcined at 400 °C	19.7364 ± 0.1592
SiC calcined at 650 °C	17.1870 ± 0.2860
SiC calcined at 850 °C	16.9450 ± 0.2682

As it can be observed, the surface area decreased by increasing the temperature of the thermal treatment. Therefore, the formation of the SiOC surface layer modifies the exposed surface area. Considering that the XRD and TEM analysis showed a substantial stability in the average size of the nanopowder before and after thermal treatments, it can be also supposed that necks could be formed between the nanograins during the thermal treatment [103]. It is well known that the decrease in the surface area negatively affects the sensitivity of a gas sensing material, because it involves a decrease of the reaction contact area between gas sensing materials and target gases [104]. Nevertheless, in the case of the thermo-activated SiC sensing film, the sensing characterization performed (section 3.2) highlighted that the improvement on the surface reactivity vs. SO_2 due to the formation of the SiOC shell prevails over the decrease in surface area, giving a further evidence of the SiC sensing performance dependence on the SiC/SiOC core-shell formation.

As in the case of metal-oxide gas sensors, the oxygen atoms adsorbed on the surface of the SiC/SiOC core-shell can be involved in the chemical reactions underlying the transduction process [105]. A possible chemical mechanism for the SO_2 detection by the SiC layer, in dry air, could be based on the oxidation of the molecule on the semiconductor surface, involving adsorbed oxygen ions and catalysed by the semiconductor itself:

$$SO_{2(g)} + O^-_{(ads)} \rightarrow SO_{3(g)} + 1e^- \quad (1)$$

$$SO_{2(g)} + O^{2-}_{(ads)} \rightarrow SO_{3(g)} + 2e^- \quad (2)$$

The electrons released from the reaction can return to the semiconductor conduction band, causing the conductivity increase of the SiC layer during the interaction with SO_2. The higher reactivity of the sensing material vs. SO_2 than the other gases analysed may lie in the working temperature of the SiC layer. On the one hand, King et al. demonstrated the possible catalytic oxidation of SO_2 to SO_3 with SiO_2 at high temperature (450-630 °C) [106]. On the other hand, a lot of works showed that, at temperatures above 550-600°C, nanostructured semiconductors result to be strongly less sensitive or insensitive to the common reducing and oxidizing gases [104, 107, 108].

Concerning the gas sensing mechanism in wet air, the presence of H_2O molecules greatly affects the reaction scenario. Indeed, water molecules can react with SO_2 in the atmosphere by producing H_2SO_3 and further by-products, before the interaction with the SiC layer [13]. Subsequently, SO_2 and the

25

other gaseous compounds, resulting from the interaction between SO_2 and H_2O, can interact with oxygen and hydroxyl ions adsorbed on the surface of the SiC/SiOC core-shell. On the one hand, this could be an additional factor that contributes to improve the sensing capabilities of the SiC sensor in wet air. On the other hand, such a complicate situation hinders the possible suppositions about the types of interaction that occur on the sensor surface.

An in-depth analysis of the interaction between the SiC-SiOC core-shell and the SO_2 molecules will require specific characterization techniques, such as IR and Raman spectroscopy measurements in OPERANDO mode, and it will be the topic of a dedicated future work.

4. Conclusions

In this work, it was demonstrated that, under proper conditions, it is possible to activate the surface reactivity of nanostructured SiC for heterogeneous interaction vs. gaseous compounds. In particular, the investigation, focused on the study of the chemoresistive sensing properties of SiC thick films in thermo-activation mode, highlighted unique sensing properties of this material, which resulted to be selective vs. SO_2 among 13 gases analysed at concentration lower than the TLV value. The electrical characterization of the tested gases showed an increase in the SiC sensing response and cross selectivity to SO_2 in the presence of humidity. In addition, the wet condition reduced the working temperature required to detect the interaction between SO_2 and SiC (550°C) compared to the dry condition (600°C). This SiC behaviour is unexpected compared to common metal-oxide gas sensors, in which the presence of humidity represents an issue, inducing a drastic decrease of the sensing response and of the sensitivity.

Further investigations showed that the enhancement of the SiC surface reactivity is promoted by the formation of a SiC-SiOC core-shell. The core-shell could catalyse the gas sensing interaction between SO_2 and the oxygen ions adsorbed on the SiOC surface, providing the increase in the SiC film conductance obtained during the gas sensing characterization. In this way, a possible mechanism of reaction has been proposed in dry air, although it will be studied deeply through suitable analysis to verify if the supposed chemical reaction really occurs.

The results obtained are worthy of attention also at the application level, given the great importance of detecting SO_2, a pollutant gaseous compound with very high toxicity for human health even at low concentrations and emitted by different industrial processes.

26

Declaration of interests

☒ The authors declare that they have no known competing financial interests or personal relationships that could have appeared to influence the work reported in this paper.

☐The authors declare the following financial interests/personal relationships which may be considered as potential competing interests:

Acknowledgments

Reference

[1] Lelieveld, J., Evans, J.S., Fnais, M., Giannadaki, D., Pozzer, A. The contribution of outdoor air pollution sources to premature mortality on a global scale (2015) Nature, 525 (7569), pp. 367-371.

[2] Chen, B., Kan, H. Air pollution and population health: A global challenge (2008) Environmental Health and Preventive Medicine, 13 (2), pp. 94-101.

[3] https://www.eea.europa.eu/themes/air/air-pollution-sources

[4] Limbeck, A., Kulmala, M., Puxbaum, H. Secondary organic aerosol formation in the atmosphere via heterogeneous reaction of gaseous isoprene on acidic particles (2003) Geophysical Research Letters, 30 (19), pp. ASC 6-1 - ASC 6-4

[5] https://ourworldindata.org/air-pollution

[6] http://www.worldbank.org/en/news/press-release/2016/09/08/air-pollution-deaths-cost-global-economy-225-billion

[7] Komarnisky, L.A., Christopherson, R.J., Basu, T.K. Sulfur: Its clinical and toxicologic aspects (2003) Nutrition, 19 (1), pp. 54-61

[8] Kazahaya, K., Shinohara, H., Uto, K., Odai, M., Nakahori, Y., Mori, H., Iino, H., Miyashita, M., Hirabayashi, J. Gigantic SO2 emission from Miyakejima volcano, Japan, caused by caldera collapse (2004) Geology, 32 (5), pp. 425-428

[9] Gschwandtner, G., Gschwandtner, K., Eldridge, K., Mann, C., Mobley, D Historic emissions of sulfur and nitrogen oxides in the united states from 1900 to 1980 (1986) Journal of the Air Pollution Control Association, 36 (2), pp. 139-149

[10] Lu, Q., Zheng, J., Ye, S., Shen, X., Yuan, Z., Yin, S. Emission trends and source characteristics of SO2, NOx, PM10 and VOCs in the Pearl River Delta region from 2000 to 2009 (2013) Atmospheric Environment, 76, pp. 11-20

[11] Xue, Y., Zhou, Z., Nie, T., Wang, K., Nie, L., Pan, T., Wu, X., Tian, H., Zhong, L., Li, J., Liu, H., Liu, S., Shao, P. Trends of multiple air pollutants emissions from residential coal combustion in Beijing and its implication on improving air quality for control measures (2016) Atmospheric Environment, 142, pp. 303-312

[12] https://www.cdc.gov/niosh/npg/npgd0575.html

[13] Meng, Z. Oxidative damage of sulfur dioxide on various organs of mice: Sulfur dioxide is a systemic oxidative damage agent (2003) Inhalation Toxicology, 15 (2), pp. 181-195

[14] Sunyer, J., Spix, C., Quénel, P., Ponce-de-León, A., Pönka, A., Barumandzadeh, T., Touloumi, G., Bacharova, L., Wojtyniak, B., Vonk, J., Bisanti, L., Schwartz, J., Katsouyanni, K. Urban air

pollution and emergency admissions for asthma in four European cities: The APHEA project (1997) Thorax, 52 (9), pp. 760-765

[15] https://www.atsdr.cdc.gov/mmg/mmg.asp?id=249&tid=46

[16] Boezen, H.M., Van Der Zee, S.C., Postma, D.S., Vonk, J.M., Gerritsen, J., Hoek, G., Brunekreef, B., Rijcken, B., Schouten, J.P. Effects of ambient air pollution on upper and lower respiratory symptoms and peak expiratory flow in children (1999) Lancet, 353 (9156), pp. 874-878

[17] Sheppard, D., Saisho, A., Nadel, J.A., Boushey, H.A. Exercise increases sulfur dioxide-induced bronchoconstriction in asthmatic subjects (1981) American Review of Respiratory Disease, 123 (5), pp. 486-491   Kampa, M., Castanas, E. Human health effects of air pollution (2008) Environmental Pollution, 151 (2), pp. 362-367

[18] Xu, Z., Xu, Z., Jing, L., Yu, D., Xu, X. Air Pollution and Daily Mortality in Shenyang, China (2000) Archives of Environmental Health, 55 (2), pp. 115-120.

[19] Katsouyanni, K., Touloumi, G., Spix, C., Schwarte, J., Balducci, F., Medina, S., Rossi, G., Wojtyniak, B., Sunyer, J., Bacharova, L., Schouten, J.P., Ponka, A., Anderson, H.R. Short term effects of ambient sulphur dioxide and particulate matter on mortality in 12 European cities: Results from time series data from the APHEA project (1997) British Medical Journal, 314 (7095), pp. 1658-1663.

[20] Schwartz, J., Dockery, D.W. Increased mortality in Philadelphia associated with daily air pollution concentrations (1992) American Review of Respiratory Disease, 145 (3), pp. 600-604

[21] Smargiassi, A., Kosatsky, T., Hicks, J., Plante, C., Armstrong, B., Villeneuve, P.J., Goudreau, S. Risk of asthmatic episodes in children exposed to sulfur dioxide stack emissions from a refinery point source in Montreal, Canada (2009) Environmental Health Perspectives, 117 (4), pp. 653-659

[22] Klimont, Z., Smith, S.J., Cofala, J. The last decade of global anthropogenic sulfur dioxide: 2000-2011 emissions (2013) Environmental Research Letters, 8 (1)

[23] https://ourworldindata.org/grapher/so-emissions-by-world-region-in-million-tonnes.

[24] Lou, X.T., Somesfalean, G., Zhang, Z.G., Svanberg, S. Sulfur dioxide measurements using an ultraviolet light-emitting diode in combination with gas correlation techniques (2009) Applied Physics B: Lasers and Optics, 94 (4), pp. 699-704

[25] Zhang, Y., Wang, Y., Liu, Y., Dong, X., Xia, H., Zhang, Z., Li, J. Optical H2S and SO2 sensor based on chemical conversion and partition differential optical absorption spectroscopy (2019) Spectrochimica Acta - Part A: Molecular and Biomolecular Spectroscopy, 210, pp. 120-125

[26] Wang, M., Guo, L., Cao, D. Amino-Functionalized Luminescent Metal-Organic Framework Test Paper for Rapid and Selective Sensing of SO2 Gas and Its Derivatives by Luminescence Turn-On Effect (2018) Analytical Chemistry, 90 (5), pp. 3608-3614

[27] Ma, C., Hao, X., Yang, X., Liang, X., Liu, F., Liu, T., Yang, C., Zhu, H., Lu, G. Sub-ppb SO2 gas sensor based on NASICON and LaxSm1-xFeO3 sensing electrode (2018) Sensors and Actuators, B: Chemical, 256, pp. 648-655

[28] Yin, X., Dong, L., Wu, H., Zheng, H., Ma, W., Zhang, L., Yin, W., Xiao, L., Jia, S., Tittel, F.K. Highly sensitive SO2 photoacoustic sensor for SF6 decomposition detection using a compact mW-level diode-pumped solid-state laser emitting at 303 nm (2017) Optics Express, 25 (26), pp. 32581-3259

[29] Liu, Y., Xu, X., Chen, Y., Zhang, Y., Gao, X., Xu, P., Li, X., Fang, J., Wen, W. An integrated micro-chip with Ru/Al2O3/ZnO as sensing material for SO2 detection (2018) Sensors and Actuators, B: Chemical, 262, pp. 26-34

[30] Septiani, N.L.W., Kaneti, Y.V., Yuliarto, B., Nugraha, Dipojono, H.K., Takei, T., You, J., Yamauchi, Y. Hybrid nanoarchitecturing of hierarchical zinc oxide wool-ball-like nanostructures with multi-walled carbon nanotubes for achieving sensitive and selective detection of sulfur dioxide (2018) Sensors and Actuators, B: Chemical, 261, pp. 241-251

[31] Van Tong, P., Hoa, N.D., Nha, H.T., Van Duy, N., Hung, C.M., Van Hieu, N. SO2 and H2S Sensing Properties of Hydrothermally Synthesized CuO Nanoplates (2018) Journal of Electronic Materials, 47 (12), pp. 7170-7178

[32] B. Yuliarto, M.F. Ramadhani, Nugraha, N.L.W. Septiani, K.A. Hamam. Enhancement of SO2 gas sensing performance using ZnO nanorod thin films: the role of deposition time. Journal of Materials Science, 52 (2017), pp. 4543-4554

[33] Çiftyürek, E., Sabolsky, K., Sabolsky, E.M. Molybdenum and tungsten oxide based gas sensors for high temperature detection of environmentally hazardous sulfur species (2016) Sensors and Actuators, B: Chemical, 237, pp. 262-274.

[34] Tyagi, P., Sharma, A., Tomar, M., Gupta, V. A comparative study of RGO-SnO2 and MWCNT-SnO2 nanocomposites based SO2 gas sensors (2017) Sensors and Actuators, B: Chemical, 248, pp. 980-986

[35] Prajapati, C.S., Soman, R., Rudraswamy, S.B., Nayak, M., Bhat, N. Single Chip Gas Sensor Array for Air Quality Monitoring (2017) Journal of Microelectromechanical Systems, 26 (2), 433-439.

[36] Gaiardo, A., Bellutti, P., Fabbri, B., Gherardi, S., Giberti, A., Guidi, V., Landini, N., Malagù, C., Pepponi, G., Valt, M., Zonta, G. Chemoresistive Gas Sensor based on SiC Thick Film:

Possible Distinctive Sensing Properties between H2S and SO2 (2016) Procedia Engineering, 168, pp. 276-279.

[37] Kim, S., Choi, J., Jung, M., Joo, S., Kim, S. Silicon carbide-based hydrogen gas sensors for high-temperature applications (2013) Sensors (Switzerland), 13 (10), pp. 13575-13583

[38] Wiche, G., Berns, A., Steffes, H., Obermeier, E. Thermal analysis of silicon carbide based micro hotplates for metal oxide gas sensors (2005) Sensors and Actuators, A: Physical, 123-124, pp. 12-17

[39] Yakimova, R., Steinhoff, G., Petoral Jr., R.M., Vahlberg, C., Khranovskyy, V., Yazdi, G.R., Uvdal, K., Lloyd Spetz, A. Novel material concepts of transducers for chemical and biosensors (2007) Biosensors and Bioelectronics, 22 (12), pp. 2780-2785

[40] Nakagomi, S., Shinobu, H., Unés, L., Lundström, I., Ekedahl, L.-G., Yakimova, R., Syväjärvi, M., Henry, A., Janzén, E., Spetz, A.L. Influence of epitaxial layer on SiC Schottky diode gas sensors operated under high-temperature conditions (2002) Materials Science Forum, 389-393, pp. 1423-1426

[41] Kim, K.-S., Chung, G.-S. Characterization of porous cubic silicon carbide deposited with Pd and Pt nanoparticles as a hydrogen sensor (2011) Sensors and Actuators, B: Chemical, 157 (2), pp. 482-487

[42] Mourya, S., Kumar, A., Jaiswal, J., Malik, G., Kumar, B., Chandra, R. Development of Pd-Pt functionalized high performance H 2 gas sensor based on silicon carbide coated porous silicon for extreme environment applications (2019) Sensors and Actuators, B: Chemical, pp. 373-383

[43] Trinchi, A., Kandasamy, S., Wlodarski, W. High temperature field effect hydrogen and hydrocarbon gas sensors based on SiC MOS devices (2008) Sensors and Actuators, B: Chemical, 133 (2), pp. 705-716

[44] Sanger, A., Jain, P.K., Mishra, Y.K., Chandra, R. Palladium decorated silicon carbide nanocauliflowers for hydrogen gas sensing application (2017) Sensors and Actuators, B: Chemical, 242, pp. 694-699

[45] Singh, N., Kumar, A., Kaur, D. Hydrogen gas sensing properties of platinum decorated silicon carbide (Pt/SiC) Nanoballs (2018) Sensors and Actuators, B: Chemical, 262, pp. 162-170

[46] Chen, J., Zhang, J., Wang, M., Li, Y. High-temperature hydrogen sensor based on platinum nanoparticle-decorated SiC nanowire device (2014) Sensors and Actuators, B: Chemical, 201, pp. 402-406

[47] Sultan, A., Ahmad, S., Mohammad, F. A highly sensitive chlorine gas sensor and enhanced thermal DC electrical conductivity from polypyrrole/silicon carbide nanocomposites (2016) RSC Advances, 6 (87), pp. 84200-84208

[48] Wang, B., Deng, L., Sun, L., Lei, Y., Wu, N., Wang, Y. Growth of TiO2 nanostructures exposed {001} and {110} facets on SiC ultrafine fibers for enhanced gas sensing performance (2018) Sensors and Actuators, B: Chemical, 276, pp. 57-64

[49] Lin, H., Gerbec, J.A., Sushchikh, M., McFarland, E.W. Synthesis of amorphous silicon carbide nanoparticles in a low temperature low pressure plasma reactor (2008) Nanotechnology, 19 (32)

[50] Kholmanov, I.N., Kharlamov, A., Barborini, E., Lenardi, C., Li Bassi, A., Bottani, C.E., Ducati, C., Maffi, S., Kirillova, N.V., Milani, P. A simple method for the synthesis of silicon carbide nanorods. (2002) J Nanosci Nanotechnol, 2 (5), pp. 453-456

[51] Chaira, D., Mishra, B.K., Sangal, S. Synthesis and characterization of silicon carbide by reaction milling in a dual-drive planetary mill (2007) Materials Science and Engineering A, 460-461, pp. 111-120

[52] Leconte, Y., Leparoux, M., Portier, X., Herlin-Boime, N. Controlled synthesis of β-SiC nanopowders with variable stoichiometry using inductively coupled plasma (2008) Plasma Chemistry and Plasma Processing, 28 (2), pp. 233-248

[53] Marc J. Madou, Stanley Roy Morrison, Chemical Sensing with Solid State Devices, the University of Michigan. Academic Press, 1989

[54] M. Wautelet, "Introduction to the Nanoworld", Key Engineering Materials, Vol. 444, pp. 1-15, 2010

[55] Yoo, J., Dayeh, S.A., Bartelt, N.C., Tang, W., Findikoglu, A.T., Picraux, S.T. Size-dependent silicon epitaxy at mesoscale dimensions (2014) Nano Letters, 14 (11), pp. 6121-6126

[56] Mattioli, G., Amore Bonapasta, A., Bovi, D., Giannozzi, P. Photocatalytic and photovoltaic properties of TiO2 nanoparticles investigated by ab initio simulations (2014) Journal of Physical Chemistry C, 118 (51), pp. 29928-29942

[57] Barreca, D., Carraro, G., Gasparotto, A., MacCato, C., Rossi, F., Salviati, G., Tallarida, M., Das, C., Fresno, F., Korte, D., Štangar, U.L., Franko, M., Schmeisser, D. Surface functionalization of nanostructured Fe2O3 polymorphs: From design to light-activated applications (2013) ACS Applied Materials and Interfaces, 5 (15), pp. 7130-7138

[58] Tsyrulnikov, P.G., Tsybulya, S.V., Kryukova, G.N., Boronin, A.I., Koscheev, S.V., Starostina, T.G., Bubnov, A.V., Kudrya, E.N. Phase transformations in the thermoactivated MnOx-Al2O3 catalytic system (2002) Journal of Molecular Catalysis A: Chemical, 179 (1-2), pp. 213-220

[59] Prades, J.D., Jimenez-Diaz, R., Hernandez-Ramirez, F., Barth, S., Cirera, A., Romano-Rodriguez, A., Mathur, S., Morante, J.R. Equivalence between thermal and room temperature UV light-modulated responses of gas sensors based on individual SnO2 nanowires (2009) Sensors and Actuators, B: Chemical, 140 (2), pp. 337-341.

[60] Gaiardo, A., Fabbri, B., Giberti, A., Guidi, V., Bellutti, P., Malagù, C., Valt, M., Pepponi, G., Gherardi, S., Zonta, G., Martucci, A., Sturaro, M., Landini, N. ZnO and Au/ZnO thin films: Room-temperature chemoresistive properties for gas sensing applications (2016) Sensors and Actuators, B: Chemical, 237, pp. 1085-1094.

[61] Gaiardo, A., Fabbri, B., Guidi, V., Bellutti, P., Giberti, A., Gherardi, S., Vanzetti, L., Malagù, C., Zonta, G. Metal sulfides as sensing materials for chemoresistive gas sensors (2016) Sensors (Switzerland), 16 (3), art. no. 296.

[62] Rodríguez-Betancourtt, V.-M., Bonilla, H.G., Flores Martínez, M., Guillén Bonilla, A., Moran Lazaro, J.P., Bonilla, J.T.G., González, M.A., De La Luz Olvera Amador, M. Gas Sensing Properties of NiSb2O6 Micro-and Nanoparticles in Propane and Carbon Monoxide Atmospheres (2017) Journal of Nanomaterials, 2017, art. no. 8792567.

[63] Giberti, A., Gaiardo, A., Fabbri, B., Gherardi, S., Guidi, V., Malagù, C., Bellutti, P., Zonta, G., Casotti, D., Cruciani, G. Tin(IV) sulfide nanorods as a new gas sensing material (2016) Sensors and Actuators, B: Chemical, 223, pp. 827-833.

[64] Fabbri, B., Gaiardo, A., Giberti, A., Guidi, V., Malagù, C., Martucci, A., Sturaro, M., Zonta, G., Gherardi, S., Bernardoni, P. Chemoresistive properties of photo-activated thin and thick ZnO films (2014) Sensors and Actuators, B: Chemical, 222, pp. 1251-1256.

[65] Sun, L., Han, C., Wu, N., Wang, B., Wang, Y. High temperature gas sensing performances of silicon carbide nanosheets with an n-p conductivity transition (2018) RSC Advances, 8 (25), pp. 13697-13707.

[66] Li, G.-Y., Ma, J., Peng, G., Chen, W., Chu, Z.-Y., Li, Y.-H., Hu, T.-J., Li, X.-D. Room-temperature humidity-sensing performance of SiC nanopaper (2014) ACS Applied Materials and Interfaces, 6 (24), pp. 22673-22679.

[67] Milovanov, Y.S., Skryshevsky, V.A., Gavrilchenko, I.V., Kostiukevych, O.M., Gryn, S.V., Alekseev, S.A. Ethanol gas sensing performance of electrochemically anodized freestanding porous SiC (2019) Diamond and Related Materials, 91, pp. 84-89.

[68] Bârsan, N., Weimar, U. Understanding the fundamental principles of metal oxide based gas sensors; the example of CO sensing with SnO2 sensors in the presence of humidity (2003) Journal of Physics Condensed Matter, 15 (20), pp. R813-R839.

[69] Hübner, M., Simion, C.E., Tomescu-Stănoiu, A., Pokhrel, S., Bârsan, N., Weimar, U. Influence of humidity on CO sensing with p-type CuO thick film gas sensors (2011) Sensors and Actuators, B: Chemical, 153 (2), pp. 347-353.

[70] Carotta, M.C., Benetti, M., Ferrari, E., Giberti, A., Malagù, C., Nagliati, M., Vendemiati, B., Martinelli, G. Basic interpretation of thick film gas sensors for atmospheric application (2007) Sensors and Actuators, B: Chemical, 126 (2), pp. 672-677.

[71] R.W. Cheary, A.A. Coelho A fundamental parameters approach to X-ray line-profile fitting, J. Appl. Crystallogr., 25 (1992), pp. 109-121.

[72] R.W. Cheary, A.A. Coelho, J.P. Cline, Fundamental parameters line profile fitting in laboratory diffractometers, J. Res. Natl. Inst. Stand. Technol., 109 (2004), pp. 1-25.

[73] A. Kern, A.A. Coelho, R.W. Cheary, Convolution based profile fitting. Diffraction analysis of the microstructure of materials, E.J. Mittemeijer, P. Scardi (Eds.), Materials Science, Springer, Germany (2004).

[74] Bruker AXS, TOPAS V4, General Profile and Structure Analysis Software for Powder Diffraction Data—User's Manual. Bruker AXS, Karlsruhe, Germany (2008).

[75] D. Balzar, Voigt-function model in diffraction line-broadening analysis R.L. Snyder, H.J. Bunge, J. Fiala (Eds.), Microstructure Analysis from Diffraction, International Union of Crystallography, New York (1999).

[76] Guidi, V., Malagù, C., Carotta, M.C., Vendemiati, B. Printed semiconducting gas sensors (2012) Printed Films: Materials Science and Applications in Sensors, Electronics and Photonics, pp. 278-334.

[77] Zonta, G., Anania, G., Feo, C., Gaiardo, A., Gherardi, S., Giberti, A., Guidi, V., Landini, N., Palmonari, C., Ricci, L., de Togni, A., Malagù, C. Use of gas sensors and FOBT for the early detection of colorectal cancer (2018) Sensors and Actuators, B: Chemical, 262, pp. 884-891.

[78] Zonta, G., Anania, G., Fabbri, B., Gaiardo, A., Gherardi, S., Giberti, A., Guidi, V., Landini, N., Malagù, C. Detection of colorectal cancer biomarkers in the presence of interfering gases (2015) Sensors and Actuators, B: Chemical, 218, pp. 289-295.

[79] Valt, M., Fabbri, B., Gaiardo, A., Gherardi, S., Casotti, D., Cruciani, G., Pepponi, G., Vanzetti, L., Iacob, E., Malagu, C., Bellutti, P., Guidi, V. Aza-crown-ether functionalized graphene oxide for gas sensing and cation trapping applications (2019) Materials Research Express, 6 (7), art. no. 075603.

[80] https://www.cdc.gov/niosh/, visited on 15th December 2018.

[81] Huguet-Garcia, J., Jankowiak, A., Miro, S., Podor, R., Meslin, E., Thomé, L., Serruys, Y. and Costantini, J. M. (2015). Characterization of the ion-amorphization process and thermal annealing effects on third generation SiC fibers and 6H-SiC. *EPJ Nuclear Sciences & Technologies*, *1*, 8.

[82] Kormányos, A., Endrodi, B., Ondok, R., Sápi, A., Janáky, C. Controlled photocatalytic synthesis of core-shell SiC/polyaniline hybrid nanostructures (2016) Materials, 9 (3), art. no. 201.

[83] Parida, B., Choi, J., Lim, G., Kim, K., Kim, K. Enhanced visible light absorption by 3C-SiC nanoparticles embedded in Si solar cells by plasma-enhanced chemical vapor deposition (2013) Journal of Nanomaterials, 2013, art. no. 953790.

[84] Dragomir, M., Valant, M., Fanetti, M., Mozharivskyj, Y. A facile chemical method for the synthesis of 3C-SiC nanoflakes (2016) RSC Advances, 6 (26), pp. 21795-21801.

[85] Charpentier, S., Kassiba, A., Bulou, A., Monthioux, M., Cauchetier, M. Effects of excess carbon and vibrational properties in ultrafine SiC powders (1999) EPJ Applied Physics, 8 (2), pp. 111-121.

[86] Kassiba, A., Makowska-Janusik, M., Bouclé, J., Bardeau, J.F., Bulou, A., Herlin-Boime, N. Photoluminescence features on the Raman spectra of quasistoichiometric SiC nanoparticles: Experimental and numerical simulations (2002) Physical Review B - Condensed Matter and Materials Physics, 66 (15), art. no. 155317, pp. 1553171-1553177

[87] Koziej, D., Bârsan, N., Weimar, U., Szuber, J., Shimanoe, K., Yamazoe, N. Water-oxygen interplay on tin dioxide surface: Implication on gas sensing (2005) Chemical Physics Letters, 410 (4-6), pp. 321-323.

[88] Barsan, N., Koziej, D., Weimar, U. Metal oxide-based gas sensor research: How to? (2007) Sensors and Actuators, B: Chemical, 121 (1), pp. 18-35.

[89] Krivec, M., Mc Gunnigle, G., Abram, A., Maier, D., Waldner, R., Gostner, J.M., Überall, F., Leitner, R.Quantitative ethylene measurements with MOx chemiresistive sensors at different relative air humidities (2015) Sensors (Switzerland), 15 (11), pp. 28088-28098.

[90] Zhang, D., Liu, J., Jiang, C., Liu, A., Xia, B. Quantitative detection of formaldehyde and ammonia gas via metal oxide-modified graphene-based sensor array combining with neural network model (2017) Sensors and Actuators, B: Chemical, 240, pp. 55-65.

[91] Urasinska-Wojcik, B., Vincent, T.A., Chowdhury, M.F., Gardner, J.W. Ultrasensitive WO3 gas sensors for NO2 detection in air and low oxygen environment (2017) Sensors and Actuators, B: Chemical, 239, pp. 1051-1059.

[92] Tan, J., Dun, M., Li, L., Zhao, J., Tan, W., Lin, Z., Huang, X. Synthesis of hollow and hollowed-out Co3O4 microspheres assembled by porous ultrathin nanosheets for ethanol gas sensors: Responding and recovering in one second (2017) Sensors and Actuators, B: Chemical, 249, pp. 44-52.

[93] Korotcenkov, G., Cho, B.K. Engineering approaches for the improvement of conductometric gas sensor parameters: Part 1. Improvement of sensor sensitivity and selectivity (short survey) (2013) Sensors and Actuators, B: Chemical, 188, pp. 709-728.

[94] Henley, R.W., Hughes, G.O. SO2 flux and the thermal power of volcanic eruptions (2016) Journal of Volcanology and Geothermal Research, 324, pp. 190-199.

[95] Kurimoto, H., Shibata, K., Kimura, C., Aoki, H., Sugino, T. Thermal oxidation temperature dependence of 4H-SiC MOS interface (2006) Applied Surface Science, 253 (5), pp. 2416-2420.

[96] Thøgersen, A., Selj, J.H., Marstein, E.S. Oxidation effects on graded porous silicon anti-reflection coatings (2012) Journal of the Electrochemical Society, 159 (5), pp. D276-D281.

[97] Newsome, D.A., Sengupta, D., Foroutan, H., Russo, M.F., Van Duin, A.C.T. Oxidation of silicon carbide by O2 and H2O: A ReaxFF reactive molecular dynamics study, part I (2012) Journal of Physical Chemistry C, 116 (30), pp. 16111-16121.

[98] Roy, J., Chandra, S., Das, S., Maitra, S. Oxidation behaviour of silicon carbide - A review (2014) Reviews on Advanced Materials Science, 38 (1), pp. 29-39.

[99] Ebrahimpour, O., Chaouki, J., Dubois, C. Diffusional effects for the oxidation of SiC powders in thermogravimetric analysis experiments (2013) Journal of Materials Science, 48 (12), pp. 4396-4407.

[100] Boyadjiev, S.I., Kéri, O., Bárdos, P., Firkala, T., Gáber, F., Nagy, Z.K., Baji, Z., Takács, M., Szilágyi, I.M. TiO_2/ZnO and ZnO/TiO_2 core/shell nanofibers prepared by electrospinning and atomic layer deposition for photocatalysis and gas sensing (2017) Applied Surface Science, 424, pp. 190-197.

[101] Karakuscu, A., Ponzoni, A., Aravind, P.R., Sberveglieri, G., Soraru, G.D. Gas sensing behavior of mesoporous SiOC glasses (2013) Journal of the American Ceramic Society, 96 (8), pp. 2366-2369.

[102] Afanas'ev, V.V., Ciobanu, F., Dimitrijev, S., Pensl, G., Stesmans, A. Band alignment and defect states at SiC/oxide interfaces (2004) Journal of Physics Condensed Matter, 16 (17), pp. S1839-S1856.

[103] Kocjan, A., Logar, M., Shen, Z. The agglomeration, coalescence and sliding of nanoparticles, leading to the rapid sintering of zirconia nanoceramics (2017) Scientific Reports, 7 (1), art. no. 2541.

[104] Wang, C., Yin, L., Zhang, L., Xiang, D., & Gao, R. Metal Oxide Gas Sensors: Sensitivity and Influencing Factors. (2010), Sensors, 10(3), 2088–2106.

[105] Yamazoe, N., Shimanoe, K. New perspectives of gas sensor technology (2009) Sensors and Actuators, B: Chemical, 138 (1), pp. 100-107.

[106] King, M. J., Davenport, W. G., & Moats, M. S. (2013). Catalytic oxidation of SO2 to SO3. Sulfuric Acid Manufacture, 73–90.doi:10.1016/b978-0-08-098220-5.00007-1.

[107] Helwig, A., Müller, G., Sberveglieri, G., Eickhoff, M. On the low-temperature response of semiconductor gas sensors (2009) Journal of Sensors, 2009, art. no. 620720.

[108] Ahlers, S., Müller, G., Doll, T. A rate equation approach to the gas sensitivity of thin film metal oxide materials (2005) Sensors and Actuators, B: Chemical, 107 (2), pp. 587-599.

Author Biographies

Andrea Gaiardo He obtained his Degree in Chemistry at the University of Ferrara in 2011 and the Master's Degree in Chemical Sciences at the University of Ferrara in 2013. He obtained the PhD in Physics on February 2018. Currently he is a Postdoc researcher involved in the field of gas sensors and micromachining.

Barbara Fabbri She obtained her master degree in Physics at University of Ferrara in 2011 and her PhD in Physics in 2015 at the same University. Currently she is a Postdoc researcher involved in the field of gas sensors and micromachining.

Alessio Giberti Bachelor in Theoretical Physics at the University of Ferrara in 2000, he obtained PhD in Physics of Matter in 2004 at the Physics Department of the University of Ferrara. His research since PhD is focused on the field of semiconductor gas sensors based on nanostructured metal oxides, with particular interest toward the electrical and selectivity properties.

Vincenzo Guidi Bachelor in Physics at the University of Ferrara in 1990, fellow at "Budker Institute for Nuclear Physics" of Novosibirsk (Russia) in 1991. Thesis of doctorate in experimental physics at Legnaro National Laboratories in 1994. Researcher in experimental physics at University of Ferrara. Research activity, carried out at the Sensors and Semiconductors laboratory of the University of Ferrara, has consisted of investigations on basic phenomena in semiconductors and top ractical implementations of sensing devices. Author of more than 140 articles in peer-reviewed journals and of more than 100 contributions to the proceedings of international conferences, reviewer and/or editors of numerous journals of Physics and Electronics, organizer of several national and international conferences and editor of the proceedings.

Cesare Malagù Bachelor in Physics at the University of Ferrara in 1997, he got his PhD in 2001 in experimental physics. Postdoc with the National Institute of Physics of Matter he received a four-year research grant starting from 2001. Fellow at the University of Wales, Swansea in 2002. Research activity, carried out at the Sensors and Semiconductors laboratory of the University of Ferrara, is mainly based on themodeling of transport phenomena in nanostructured semiconductors.

Matteo Valt is a chemistry student at university of Ferrara, actually working on a Master's degree thesis in chemoresistive gas sensors at department of physics focusing on graphene based materials for gas sensing Author Biographies application. He is a PhD Student in Physics since November 2016 at University of Ferrara.

Sandro Gherardi Bachelor in Physics Technologies at the University of Ferrara in 2002. Research activity carried out at the Sensors and Semiconductors laboratory of the University of Ferrara about gas sensing and industrial applications of monitoring devices by nanostructured semiconductor based sensors.

Giulia Zonta She received the Bachelor's Degree in Physics and Astrophysics in December 2010 (110/110 cum laude) and the Master's Degree in Physics in October 2013 (110/110), at the University of Ferrara. In January 2014 she started her Ph.D. in Matter Physics, working with the Sensors Team, coordinated by Dr. Cesare Malagù. In theApril ofthe same year she obtained the recognition "Ferrara School of Physics", that rewards the internationality of her Master's thesis work. Currently her research focuses on the study of the physic-chemical behavior of chemoresistive nanostructured gas sensors, put in contact with volatileorganic compounds (VOCs) of medical interest. With her team she won Unife Cup2013, a business plan competition that rewards innovative start-ups and StartCup Emilia Romagna 2014, with the objective to create a start-up for the realization of devices for medical screenings. Now she is the co-supervisor of two students which are working for the Bachelor's and Master's Degree in Physics respectively.

Nicolo Landini was born in Bentivoglio (BO), Italy, in 01/09/1987. He has attained the Master's Degree in Physics on 18/12/2014 at the University of Ferrara, with a thesis aimed to the study of tumor markers with

nanostructured sensors, combining for this research solid state and soft matter physics. He is a PhD Student since 28/09/2015 in the same university, under Dr. Cesare Malagù mentorship.

Giuseppe Cruciani Full Professor of Mineralogy at the University of Ferrara. Graduate with honor in Geological Sciences in 1993 at the University of Perugia, there he got a PhD in Mineralogy (Crystallography) and Petrology in 1989. Visiting scientist in 1995 at the European Synchrotron Radiation Facility (ESRF) in Grenoble, France. Member 2008- 2010 of the chemistry review committee for project selection at ESRF, still in the proposal review panel for hard condensed matter-structures at the Elettra synchrotron in Trieste, Italy. Past President 2012-2013 of the Italian Society of Mineralogy and Petrology, is Associate Editor of the European Journal of Mineralogy. Major research fields in crystallography and crystal-chemistry of zeolite-like minerals and their synthetic analogues, and of many other silicate and oxide systems. Experimental skills mostly focused on single crystal and powder diffraction, both with conventional X-rays and large scale facility radiation (synchrotron X-rays and neutrons)

Davide Casotti Bachelor in Geology at the University of Ferrara in 2010. He got his PhD In 2017 in Physic and Nanosciences at University of Modena and Reggio Emilia. He received research grants from 2010 to 2013 and from 2017 to 2018 at the University of Ferrara. Currently, he is working at INFN - section of Ferrara. Research activity is mainly based on nanomaterials (powders and films) for gas sensors and TCO-films.

Pierluigi Bellutti He received his Physical-Chemistry Laurea degree in 1984 and then started his research activity in silicon microtechnology, mainly on CCD and CMOS technologies. From 2000 till 2013 has been managing the MicroTechnologies Lab at FBK, in which R&D and production of new types of silicon radiation sensors and MEMS, are carried out. Since January 2014 he is managing the MNFacility, where the Microtechnologies activities have been joined with those of Material Characterization.

Lia Vancetti obtained her Solid State Physics at the University of Parma in 1985. She specialized in Materials Science in 1988 at the Physics Department of the University of Parma. From 1990 to 1992 she joined, as a postdoctoral associate, the University of Minnesota, Chemical Engineering and Materials Science department, working on electron spectroscopy (X-ray and Synchrotron sources). She is currently employed as a researcher at FBK, Trento. Her research since 1995 is focused on the field of x-ray photoelectron spectroscopy (XPS) using this technique on a wide variety of samples and aplications, ranging from microelectronics, to sensors, to biomedicals.

Evgeny Demenev obtained master degree in quantum optics in 2009 at the Novosibirsk State University. Since receiving PhD degree in Material Science in 2013 at University of Trento, his work as experimental physicist has been focused mainly on rapid device prtotyping and integration of silicon-based semiconductor devices, with particular accent on si-based X-Ray and nanostructured metal oxides gas sensors.